Thesis for the degree of Master of Engineering

A Hybrid Control Method of MMC-Based PV and BESS Under Uneven Irradiation

Tran Thai Nguyen

Faculty of Applied Energy System
Electrical Engineering Major
The Graduate School
Jeju National University

August 2023

A Hybrid Control Method of MMC-Based PV and BESS Under Uneven Irradiance

A Thesis submitted to the graduate school of
Jeju National University in partial fulfillment of
the requirements for the degree of Master of Engineering
under the supervision of Professor Yeong-Jun Choi

The thesis for the degree of Master of Engineering
by Tran Thai Nguyen
has been approved by the dissertation committee

August 2023

Chair	**Prof. Gae-Myoung Lee**
Member	**Prof. Young Gyu Jin**
Member	**Prof. Yeong-Jun Choi**

A Hybrid Control Method of MMC-Based PV and BESS Under Uneven Irradiance

Tran Thai Nguyen

Faculty of Applied Energy System
Electrical Engineering major
The Graduate School
Jeju National University

Abstract

In the trend of renewable energy, Photovoltaic (PV) energy with PV plants are invested rapidly. Due to the natural fluctuation of irradiation, getting the Maximum Power Point Tracking (MPPT) algorithm and balancing power output are achieving points. This thesis proposed the modified topology of a hybrid Modular Multilevel Converter (MMC) - based PV- Battery Energy Storage System (BESS). By using the individual SM capacitor voltage, PV arrays could be adopted at Maximum Power Point (MPP) voltage without DC/DC converters when interfacing with Sub-Modules (SMs). BESSs are the solution applied in this proposed topology to eliminate power mismatching under partial shading conditions. To guarantee the applicability of the system, PSCAD/EMTDC software is used to make the simulations according to uneven illumination conditions. By adopting the method, the power mismatching is reduced by BESSs' power exchanging with Total Harmonic Distortion (THD) under 5%.

부분 음영 하에서 MMC 기반의 태양광 발전 및 BESS를 위한 하이브리드 제어 방법

Tran Thai Nguyen

제주대학교 대학원

에너지응용시스템학부 전기공학전공

요약

재생 에너지의 트렌드에 따라 PV 발전소와 함께 PV 에너지에 대한 투자가 급속히 이뤄지고 있다. 일사량의 자연적인 변동으로 인해 최대 전력점 추종(MPPT) 알고리즘과 출력 밸런싱은 중요한 요소이다. 본 논문에서는 하이브리드 모듈형 다단계 변환기(MMC) 기반의 PV-배터리 에너지 저장 시스템(BESS)의 수정된 토폴로지와 제어법을 제안한다. 제안한 방식은 BESS를 활용하여 부분 음영 조건에서 전력 불일치를 제거하기 때문에, 개별 서브모듈(SM)은 DC/DC 컨버터 없이 PV 어레이를 최대 전력점(MPP) 전압에서 운전할 수 있다. 시스템의 유효성을 검증하기 위해, PSCAD/EMTDC 소프트웨어를 사용하여 불균일한 일사량 발생 시의 조건에서 시뮬레이션을 수행하였다. 검증결과 제안한 방식의 총 고조파 왜율(THD)이 5% 미만을 달성하고, 기존 방식에 비하여 부분음영에 강인하여 레그 간 전력 불균형이 감소함을 확인하였다.

Acknowledgement

This study would not have been completed without assistance from special people throughout my Master's journey. Therefore, I would like to extend my sincere gratitude to all of them.

I would like to express my deepest gratitude to my supervisor – Prof. Yeong-Jun Choi for all of his helps about financial support, encouragement, invaluable materials and constructive advice throughout my thesis journey. I highly appreciated his encouragement and timely support.

I would like to thank to another Prof Eel-Hwan Kim for directing me to come Jeju National Unitversity. I would not have studied here without his helps.

I would like to extend my thanks to other Professors at Department of Electrical Engineering, Prof. Gae Myoung Lee, Prof. Se Ho Kim, Prof. Ho Chan Kim, Prof. Ho Min Kim, Prof. Young Gyu Jin for teaching me during the Master's course. In particular, they have provided me with profound knowledge, useful pieces of writing, advice on research ideas. Their direction helped me to broaden my view and knowledge.

I am grateful to everyone in our group at the Power Electronics Lab for sharing information and providing warm assistance. Moreover, their insightful comments and encouragement; stimulating discussions, and the fun we have had during the last three years.

I owe my heartfelt thanks to my family in Viet Nam for their endless love, care and unflagging support all the time. Besides, my girlfriend is an important person who is my companion to share in stressful times as well as difficult times, she always encouraging me to increase my motivation.

Abbreviations

MMC	Multilevel Modular Converter
SM	Sub-module
MPPT	Maximum Power Point Tracking
IGBT	Insulated Gate Bipolar Transistor
PV	Photovoltaic
BESS	Battery Energy Storage System
HVDC	High Voltage Direct Current
PS modulation	Phase – Shift modulation
NZS	Net Zero Scenario
IEA	International Energy Agency
THD	Total Harmonic Distortion
DoD	Deep of Discharge
MAF	Moving Average Filter

List of symbols

N	Number of submodules in each arm
U_{DC}^{*} , U_{DC}	Reference and measured DC-link voltage, respectively
U_{PV}	PV array voltage
$\overline{U}_{PV}$	Average voltage of all PV arrays in the leg
U_{MPPT}	MPPT voltage of PV array
$\overline{U}_{MPPT}$	Average value of all MPPT voltages of PV arrays
u_{t_u}	Phase voltage in the equivalent circuit of MMC
u_{td}, u_{tq}, u_{sd}, u_{sq}	dq-axis components of the voltage
i_d, i_q	dq-axis components of current
u_{up}, u_{low}	Upper and lower arm voltages, respectively
i_{up}, i_{low}	Upper and lower arm currents, respectively
i_{cir_u}	Circulating current of phase *u (u = A, B, C)*
$u_{ref1\_u}^{*}$	Output of leg average voltage control of phase *u*
$u_{ref2\_uj}^{*}$	Output of individual voltage control for PV-SM *j*-order in phase *u*
$u_{PV\_uj}^{*}$	Final reference of PV-SM order *j* in phase *u*
$U_{BESS\_k}^{*}$	Voltage reference of the DC/DC converter of BESS
$P_{MAF}(t)$	Output power after MAF
P_{O_i}	Power point in the window size of the MAF method
P_{BESS}^{MAF}	Power reference of each BESS
P_{arm_avg}	Arm average power of the system
P_{arm_n}	*n*-th arm power
$P_{BESS\_k}^{AVG}$	Power reference of each BESS after arm power mismatching elimination

$P^{*}_{BESS\_k}$	Final reference of each BESS
L_{arm}	Arm inductor
L	Lilter inductor
R	Filter resistor
Δu_c	Variation of SM capacitor voltage
C	SM capacitor
i_{PV}	PV array current
i_{SM}	SM current
i_{CSM}	SM capacitor current
i_{BESS}	BESS current
ω	Fundamental angle frequency
S	Apparent power
W_{arm}	Arm energy
W_{SM}	SM energy
m_v	Modulation index
φ	Corresponding phase angle
U_{RMS}	RMS value of output voltage
ε	Ripple range of SM capacitor voltage
Q_{loss}	Loss of battery capacity
t	Cycling time
T	Temperature
$Rate$	Discharge rate
P_{BESS}	BESS power
E_{BESS}	Battery energy
Δt	Time interval

R_x, R_y	Two ranges are calculated from the three first points of the datasheet of DoD
RF	Rainflow cycle
D_{RF}	Rainflow degradation
$D_{calendar}$	Calendar degradation
D_{LT}	Annual degradation
I_m	Irradiation

Contents

List of Figures ..... **x**

List of Table ..... **xi**

Chapter 1. Introduction **1**

1.1. Motivation of the thesis 1

1.2. Knowledge background 2

1.3. Purpose of the thesis 7

1.4. Thesis layout 8

Chapter 2. Hybrid MMC – Based PV And BESS **9**

2.1. Structure of hybrid MMC – Based PV and BESS 9

2.2. Mathematical model of the hybrid system 10

2.3. Sub-module operation states 12

2.4. Design of the system 15

2.4.1. Design of the arm inductor 15

2.4.2. Design of the submodule capacitor 16

2.4.3. Design of BESS 17

Chapter 3. Control of the hybrid MMC – based PV and BESS **22**

3.1. Grid-connected control 22

3.2. PV – SM capacitor voltage balancing 23

3.2.1. PV – SMs leg average voltage control 24

3.2.2. Individual voltage control 25

3.3. BESS control scheme 27

3.3.1. Smooth power control 27

3.3.2. Power mismatching elimination 28

Chapter 4. Simulation Results 30

4.1. The power smoothly..... 31

4.2. Arm power mismatching elimination..... 35

Chapter 5. Conclusion 39

References..... 41

List of Figures

Fig 1.1 Configuration of PV systems 3

Fig 1.2 The hybrid MMC – PV system 5

Fig 1.3 The hybrid MMC – PV and BESS system 6

Fig 2.1 The overview of the hybrid MMC – based PV and BESS 9

Fig 2.2 Single phase MMC. 11

Fig 2.3 Working states of PV – SM. 13

Fig 2.4 Working states of BESS – SMs. 14

Fig 2.5 Battery Cycle Life as a function of DoD 19

Fig 3.1 The overall grid-connected control of the MMC – based PV and BESS system. 23

Fig 3.2 The individual PV – SM capacitor voltage balancing algorithms 26

Fig 4.1 The simulation systems 30

Fig 4.2 The irradiation data and output power of both systems in the fluctuation of irradiation condition. 33

Fig 4.3 The SM voltages of the proposed system 34

Fig 4.4 The THD of both systems in the fluctuation of irradiation condition 35

Fig 4.5 The irradiation data and output power in the partial shading condition 36

Fig 4.6 The arm power of both systems 37

Fig 4.7 The THD of both systems in partial shading condition 38

List of Table

Table 4. 1 The MMC system parameters 31

Table 4. 2 The PV – SM parameters 31

Table 4. 3 The Controller parameter 32

Chapter 1. Introduction

1.1. Motivation of the thesis

The current industrial development experienced 4 times of revolutions with the attendance of electric machines from the second from 1871 to 1914. Therefore, the development of load demand and generators have increased incessantly. Following the historical data collected by the International Energy Agency (IEA), electric consumption has increased yearly, it reached about 25 000 TWh in 2019 and more than 2.5 times compared to 20 years before [1]. To respond to load development, the energy generator plants were built with the promotion of the industry. According to the data, the contribution of many kinds of sources increases the total generation of power it satisfies the load demand with the main supply from coal, natural gas, and hydro energy with the total generation reaching 27 044 TWh in 2019.

Besides the rapid development of industry, global warming is an alert to environmental problems. This is from many harmful agents with CO_2 emission being one of the main factors that have been mentioned in a lot of reports about global warming and greenhouse gas emission. As the report comes from Our World in Data, the CO_2 emission from fossil fuels and industry has increased suddenly from the 40^{th} to the 50^{th} of the last century, the application of electric machines in the industry (the second industrial revolution) and the peak reached 36.7 billion tons in 2019 [2].

Besides the traditional sources (coal, oil, natural gas, nuclear, hydro,…), green energy (wind, solar,..) starts to be focused on its advantages (numerous environmental benefits – non-CO_2 emission). In other to contribute to making slow into global warming processing, many governments, and non-governmental foundation about the environment with attendance from many countries in the world, they propose policies and standards for production activities. Following that, the environmental problems are controlled, CO_2 emissions especially. Besides

new consensus about production activities, green energy sources have been discussed and promoted. Representatively, IEA is the foundation, which directs energy development with the combination of countries and industries, IEA incorporates more than 40 countries that approve efforts and a fighting chance of reaching net zero emissions by 2050 and limiting the increase in global temperatures to 1.5 °C. One of the representative proposals is changing traditional energy sources to renewable energy with the purpose, of the share of renewable energy in total generation raising to over 60% in 2030 and near by 90 % in 2050. Following that, Solar PV and Wind energy are the main factors, they make increasing the renewable energy contribution. They are directed at about 32.3% and 34.5% in 2030 for solar and wind energy, respectively. That is the motivation for the study of renewable energy with solar energy as this thesis.

1.2. Knowledge background

Based on the demand and direction for renewable energy development, PV Solar is one of the interesting sources. Taking that trend, this thesis is conducted to contribute to the development of PV Solar plants as well as decreasing CO_2 emissions.

With the investment from governments and energy cooperation in the world, PV plants have been built increasingly for the diversity of amount and capacity. Among that, reaching high effectiveness of PV panels, structures of converters have been designed to be suitable for levels of PV plants' capacity. It consists of four types of converters such as microinverter (in 50 - 500 Wp – range for only one PV panel), string inverters (in 0.4 - 2 kWp - range for small plants in one string), multi-string inverters (in 1.5 - 150 kWp – range for medium to large plants in several strings), and central inverters (in 80 - 4000kW – range for medium to large scale, and modular design for hundredths of a MWp) [3-6]. Fig 1. 1 shows the structure of four types of converters. Following that, DC/DC converters achieve the Maximum Power Point Tracking (MPPT) function, which is approaching maximum power from PV panels/arrays.

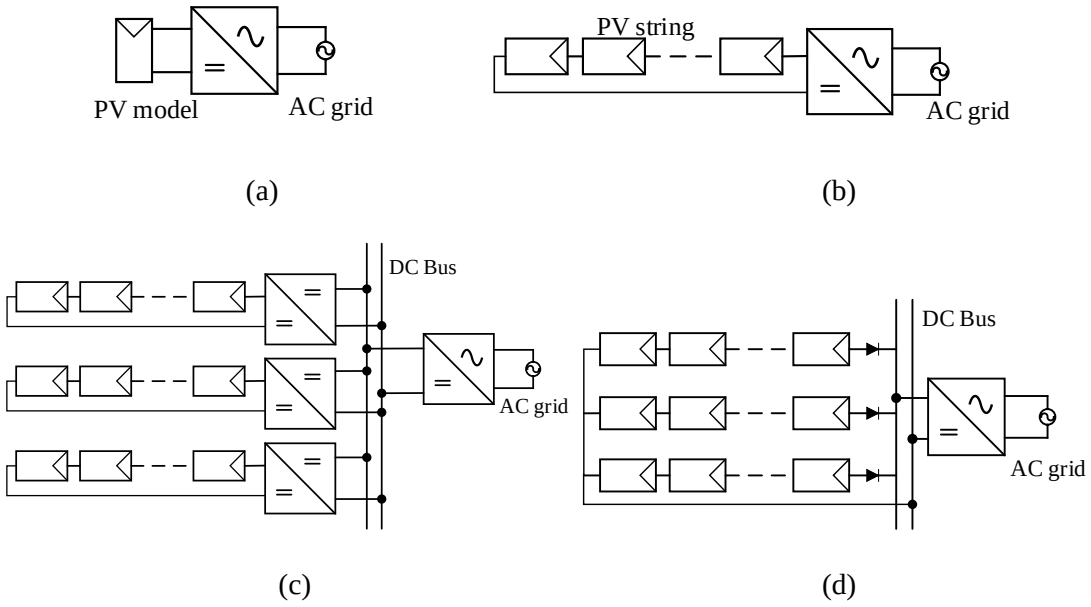

Fig 1.1 Configuration of PV systems: (a) microinverter; (b) string inverter; (c) multi-string converter; (d) central inverter.

Besides raising small and medium plants from civil (household systems), investment in medium to large PV plants has been encouraged to approach more contributions to total electric generation. In which the multi-string and central inverters have taken the advances with the central inverter being the most useful in this case. Due to the many advantages of robust and easy structure with convenient operation by a simple control and structure. Besides, this type consists of some problems for poor power factor and high harmonic in the output [7]. Therefore, the efficiency is not high as well as more losses than the types for smaller scales. This is the chance to research topics about converters for large scale plants. In many studies, a multilevel converter is one of the solutions considered with a Modular Multilevel Converter (MMC) as a promising candidate.

The MMC is one kind of the best multilevel converters for more enhanced advantages. It was proposed originally by Prof.Maquardt in 2001 [8]. The MMC is considered to use in this paper due to its preeminent characteristics, low harmonic distortion, and low sub-module voltage is there. Besides, it is possible to connect to the main grid directly, which means fewer expenses with no fee for transformers. Therefore, MMC was developed rapidly to apply

industrial widely. Nowadays, MMC systems have already been applied successfully for High Voltage Direct Current (HVDC) in China, Europe, and the USA in point-to-point, multi-terminal and hybrid systems [9]. Besides, some manufacture product MMC components and technology such as SIEMENS, Hitachi-ABB, CEPRI, and GE (formerly Alstom) [10-12]. In addition, the application of MMC is not only conducted for high voltage, but it also applies to low voltage converters because of the many advantages mentioned. Taking the advance of that trend, MMCs have been researched to contribute to renewable energy in some fields like BESS, PV, and a combination of them [13-26].

In terms of system design for PV plants by MMC application, some configurations are released and they are shown in Fig 1.2. As the other converters, an MMC is used as a main DC/AC converter for the PV array through the MPPT DC/DC converter in Fig 1.2 (a) as well as the other inverters in Fig 1.1. Into that topology, PV and DC/DC converters could be replaced by topologies of string or multi-string topology, respectively. In addition, new topologies have been conducted and released as two typical topologies in Fig 1.2 (b) and (c). They show the MMC – PV system with the highlight, which consists of many separated PV arrays depending on the number of SMs in MMC instead of the amount of all PV panels in Fig 1.2 (a). Unlike the configuration in Fig 1.2 (a) with poor MPPT, the configuration in Fig 1.2 (b) with more PV arrays and MPPT DC/DC converters respectively could be harvested energy with more effectiveness. Due to distributed control for each PV array, thus the topology is available to reduce poor MPPT under partial shading conditions of illumination. The configuration in Fig 1.2 (c) shows the new topology for the MMC – PV system without DC/DC converter between PV arrays and SMs, therefore it switching loss from DC/DC converters is eliminated.

Although the benefits of green energy, PV plants exist some advantages with output fluctuation because of natural unevenness from irradiation. Thus, compensation from Battery Energy Storage System (BESS) is considered the optimal solution currently. To compensate for the power ripple from PV plants, BESS could be placed nearby the plants with the coupled

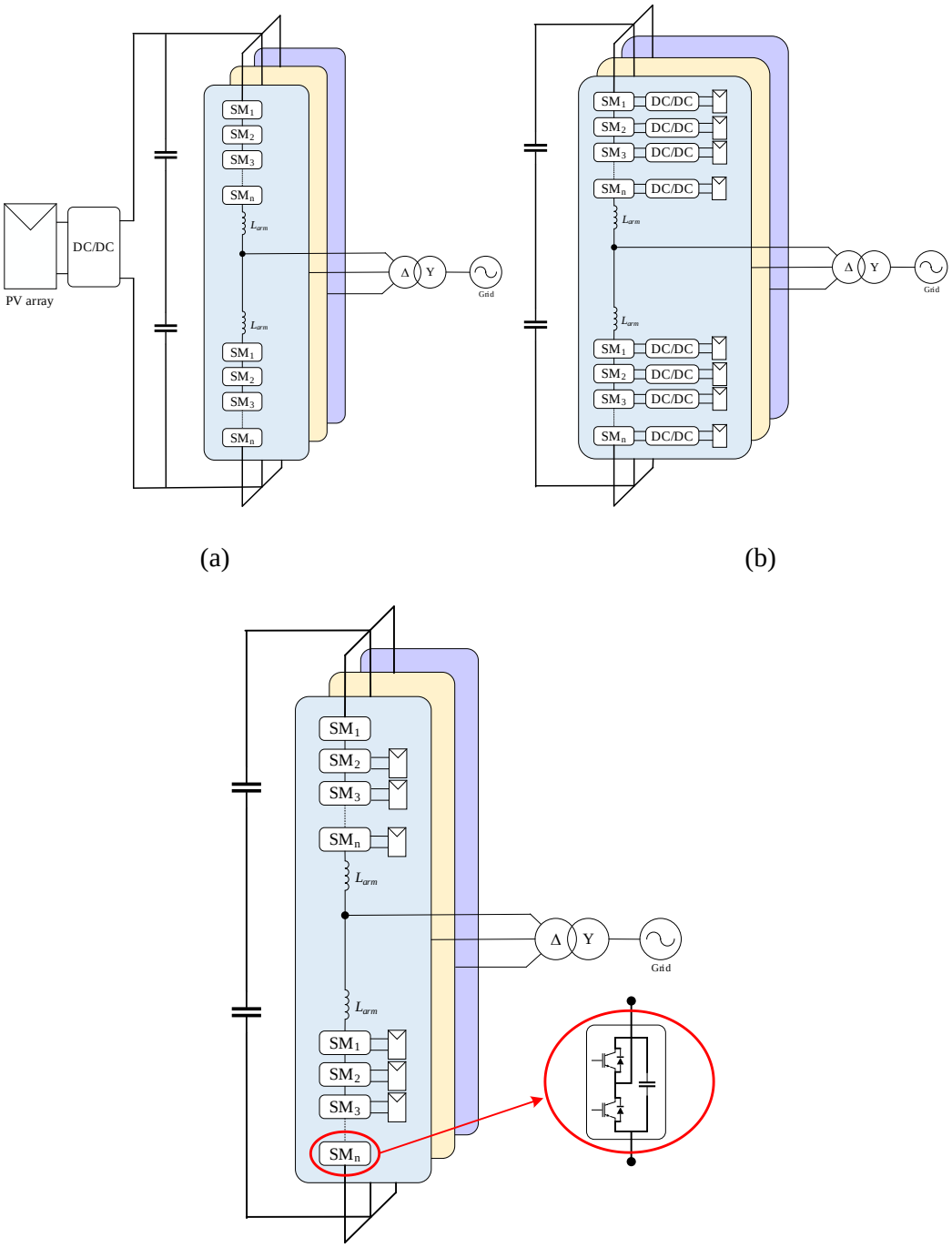

(a) (b)

(c)

Fig 1.2 The hybrid MMC – PV system.

or separated structure from the plants. Fig 1.3 lists some typical hybrid MMC – PV and BESS systems in some research studies [16-25]. The most common topology is the system in Fig 1.3 (a), BESS is placed in the DC common point of MMC, this topology allows to approach of MPPT distribution and mismatching power compensation by BESS. The other topology

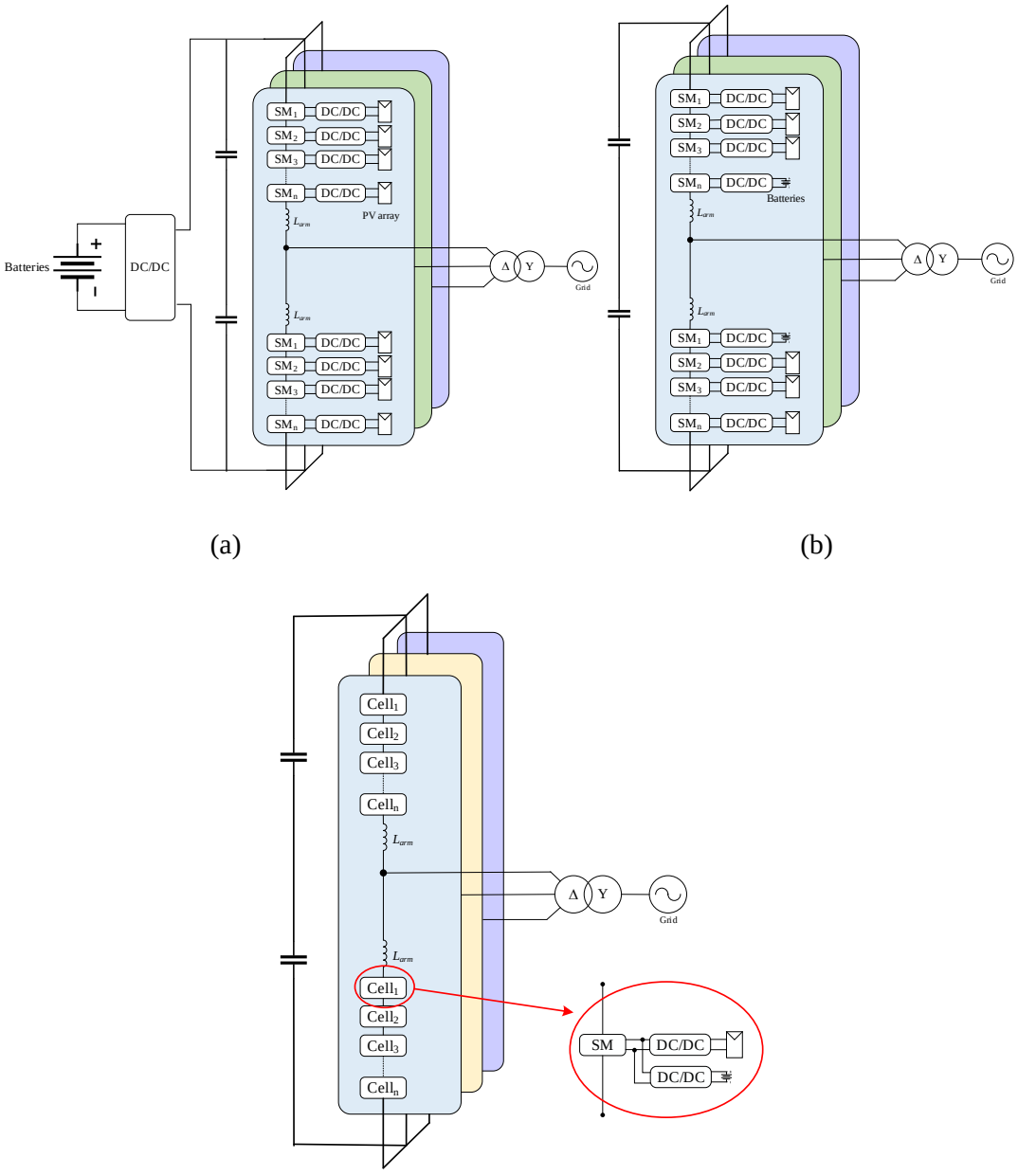

(a) (b)

(c)

Fig 1.3 The hybrid MMC – PV and BESS system

with a separated BESS topology is released in Fig 1.3 (b). Besides approaching MPPT distribution for each PV array, one BESS interfaced to an SM in the MMC structure is a new point in this study literature. Its advantages consist of the elimination of arm power mismatching and output fluctuation. Following this topology, only one BESS is connected to an arm, therefore the power compensation is limited by SM power per arm or 6 times SM power in the system. To adopt this limitation, the topology in Fig 1.3 (c) is published with

strong points, one of the innovations is the contribution of BESS in each SM. Thus, compensated power could be surpassed the limitation compared to the configuration in Fig 1.3 (b). According to the topologies in Fig 1.3, they consist of many DC/DC converters. Therefore, switching loss is their disadvantage and weak point that need to be improved.

1.3. Purpose of the thesis

Due to the motivation above, this thesis's purpose is to release a method besides modified topology. This thesis proposes a modified topology with the hybrid MMC – Based PV and BESS, which could reduce switching loss from many DC/DC converters, eliminate arm power mismatching, and adopt a control method, respectively.

The modified structure takes advances from structures in Fig 1.2 (b) and Fig 1.3 (b). The modified structure is described in the next chapter as shown in Fig 2.1. Total PV panels are separated into PV arrays, each part connects to the DC side of MMC SM directly, and BESSs are divided into multiple of 6 respective to the number of BESS per arm. Therefore, it could be inherited their advantages included MPPT approaching per each PV array without DC/DC converter, arm power mismatching elimination, and less switching loss than the other topologies. Moreover, the proposed system overcomes the BESS power limitation in the topology in Fig 1.3 (b) when it is attacked with more BESS in one arm instead of one BESS per arm. Thus, power compensation could reach a larger value that is respective to BESS charge/discharge power per arm. Depending on the power compensation, the circulating current and THD of output get low.

To adopt the topology, the control method is proposed to be suitable under variable working conditions. In this method, each PV array is run under MPP voltage during working based on individual SM voltage control. Besides, the Moving Average Filter (MAF) is applied to eliminate natural fluctuations of irradiation, and arm power mismatching control contributes to reducing the mismatching power for each arm under partial shading.

In this thesis, the BESS capacity estimation is presented as well as the reference to estimate the BESS capacitor with the optimized long-life based on Discharged rate, calendar fade estimation, and Rainflow algorithms.

To demonstrate the working ability of the proposed system, the simulations are conducted under near-realized conditions. Therefore, a constant value of irradiance is excluded. Instead, uneven irradiation conditions such as fluctuation of irradiation and partial shading, are considered as two main factors condition in the simulation that is shown in Chapter 4. For both cases of simulations, the system is possible to approach MPPT per PV arrays and IEEE standard of harmonic for the grid-connected converter [27]. PSCAD simulator is used to provide results for simulations in this thesis.

1.4. Thesis layout

Chapter 2 describes the conventional and the hybrid MMC – Based PV and BESS structure. Besides, the parameters calculated method are presented.

Chapter 3 describes the control strategy.

Chapter 4 gives the simulation results for 2 common study cases.

Chapter 5 draws the conclusion

Chapter 2. Hybrid MMC – Based PV And BESS

2.1. Structure of hybrid MMC – Based PV and BESS

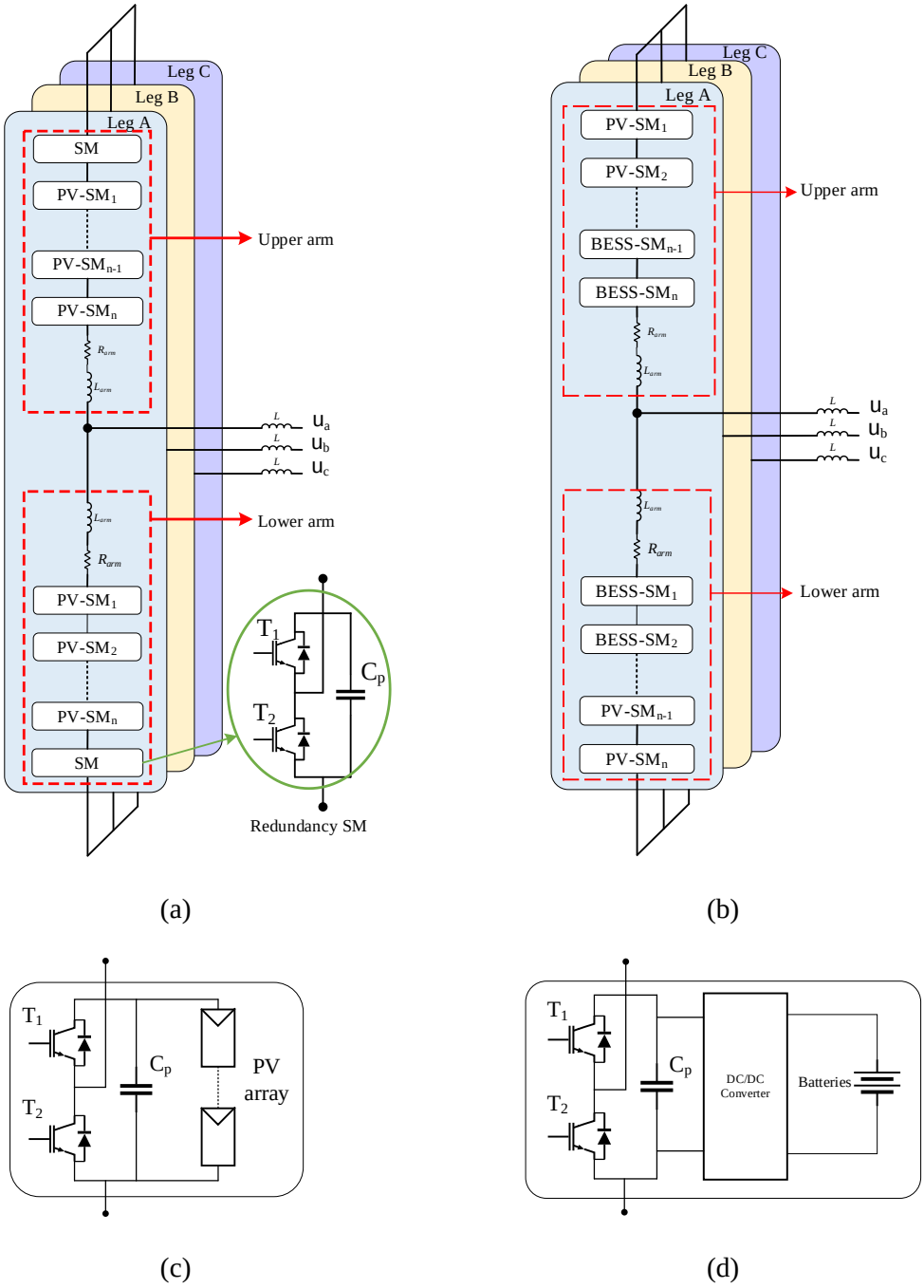

Fig 2.1 The overview of the systems; (a) The conventional system; (b) The hybrid MMC – based PV and BESS; (c) PV – SM structure; (d) The BESS – SM structure.

Fig 2. 1 (a) shows the conventional structure of the MMC – based PV [24]. The system structure consists of three legs, each leg includes 2 arms – the upper arm and lower arm, respectively. Each arm consists of SMs connected in a series and a series inductor which supports current control and limits current fault as shown in Fig 2.1 (a). A SM is a half-bridge cell that consists of two Insulated Gate Bipolar Transistors (IGBTs), two anti-parallel diodes, and a capacitor they are connected to a PV array as PV – SM (it is shown in Fig 2.1 (c)), and without PV arrays as a redundancy submodule.

The hybrid MMC – Based PV and BESS system is applied in this thesis which is presented in Fig 2.1 (b) in detail. Familiar with the conventional structure, the hybrid system consists of PV – SMs and BESS – SMs (a SM connected to batteries through a DC/DC converter), it is shown in Fig 2.1 (d)). Following the structure, the number of PV – SMs depended on the rated power of the PV plant, and the number of the BESS – SMs depended on the requirements of compensated power. The level of the system is related strictly to the number of SMs per arm. If an arm consists of N SMs, which is respective to $N + 1$ level MMC. During working time, there are always N SMs at the ON state and N SMs at the OFF state. Thus, DC-link voltage could be the constant value at any time.

To evaluate the operability of the proposed method, both structures are configurated with their control for the simulation that is presented in Chapter 4.

2.2. Mathematical model of the hybrid system

To design the control system and analysis of the MMC internal power flow, the mathematical model of MMC. Thus, a single-phase equivalent MMC is established instead of a complex for full MMC in detail. Fig 2.2 shows the single-phase equivalent circuit of the system. As seen in Fig 2.2, the mathematical model of the system is given by (1).

$$\begin{cases} 2u_{t\_u} = (u_{up} - u_{low}) + L_{arm}\dfrac{d\ \ i_{up} - i_{low}}{dt} \\ i_u = i_{up} - i_{low} \\ i_{cir\_u} = \dfrac{i_{up} + i_{low}}{2} \end{cases} \tag{1}$$

Where u_u and i_u are the output voltage and current of phase *u* with *u* = *a*, *b*, *c*. u_{up}, i_{up} and u_{low}, i_{low} are voltage and current of the upper and lower arm, respectively. And i_{cir} is the circulating current phase *u*, it is presented in the early of this section. According to (1), the output voltage and DC-link voltage could be given by (2).

$$\begin{cases} u_{t\_u} = \dfrac{1}{2}\ u_{up} - u_{low}\ + \dfrac{1}{2}L\dfrac{di_u}{dt} \\ U_{DC} = \ u_{up} + u_{low}\ + 2L\dfrac{di_{cir\_u}}{dt} \end{cases} \tag{2}$$

Assuming:

$$\begin{cases} e = \dfrac{1}{2}\ u_{up} - u_{low} \\ u_{cir\_u} = L\dfrac{di_{cir\_u}}{dt} \end{cases} \tag{3}$$

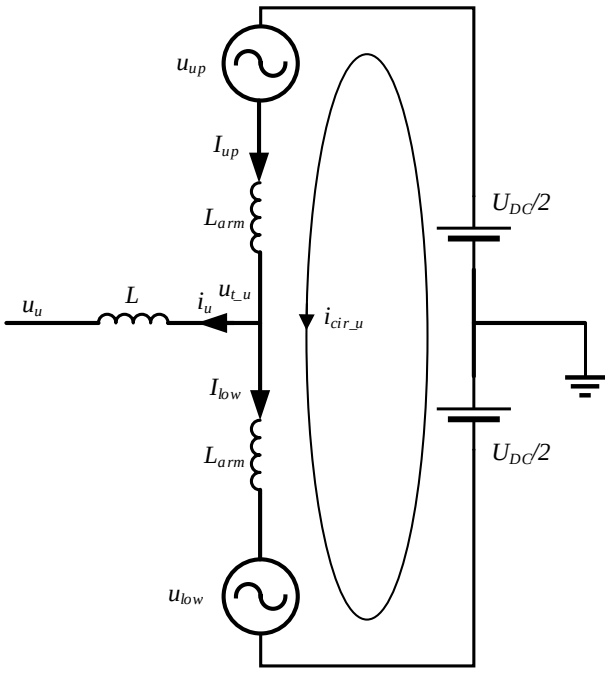

Fig 2.2 Single phase MMC.

Then, u_{t_u} could be given by (4).

$$u_{t\_u} = e + \frac{1}{2} L \frac{di_u}{dt} \tag{4}$$

The combination between (2) and (3), The upper and lower voltage are expressed by:

$$\begin{cases} u_{up} = \frac{1}{2} U_{DC} - e - u_{cir\_u} \\ u_{low} = \frac{1}{2} U_{DC} + e - u_{cir\_u} \end{cases} \tag{5}$$

2.3. Sub-module operation states

There are two types of SMs in the proposed topology with PV – SM and BESS – SM, respectively. Due to their characteristics, the PV – SMs with PV arrays transform solar energy into electric energy, and BESS – SMs approach to compensate for the arm voltage and power by their charging and discharging power. Fig 2.3 and Fig 2.4 illustrate the working states of PV – SMs, and BESS – SMs, respectively. The conduction paths of the SMs depended on whether the IGBTs needed to be on or off along with the polarity of the current.

Following the PV – SM operation in Fig 2.3, which is summarized as:

State I: T_1 is switched ON and T_2 is switched OFF, the SM voltage equals the capacitor voltage. If the SM current i_{SM} flows into the SM as shown in Fig 2.3 (a), the SM capacitor will be charged through the anti-parallel diode D_1 by i_{SM} and PV array i_{PV}. Oppositely, if the SM current flows out of the SM, the SM capacitor will be charged or discharged depending on the PV array current as shown in Fig 2.3 (b) and (c). In this state, the SM voltage is equal to the capacitor voltage, and the variation of SM capacitor voltage ΔU_C is given by (6).

$$\Delta U_C = \frac{1}{C} \int i_{PV} - i_{SM} \, dt \tag{6}$$

State II: T1 is switched OFF and T2 is switched ON, depending on the SM current directions, the SM current will pass through T2 or D2 as shown in Fig 2.3 (d) and (e), respectively.

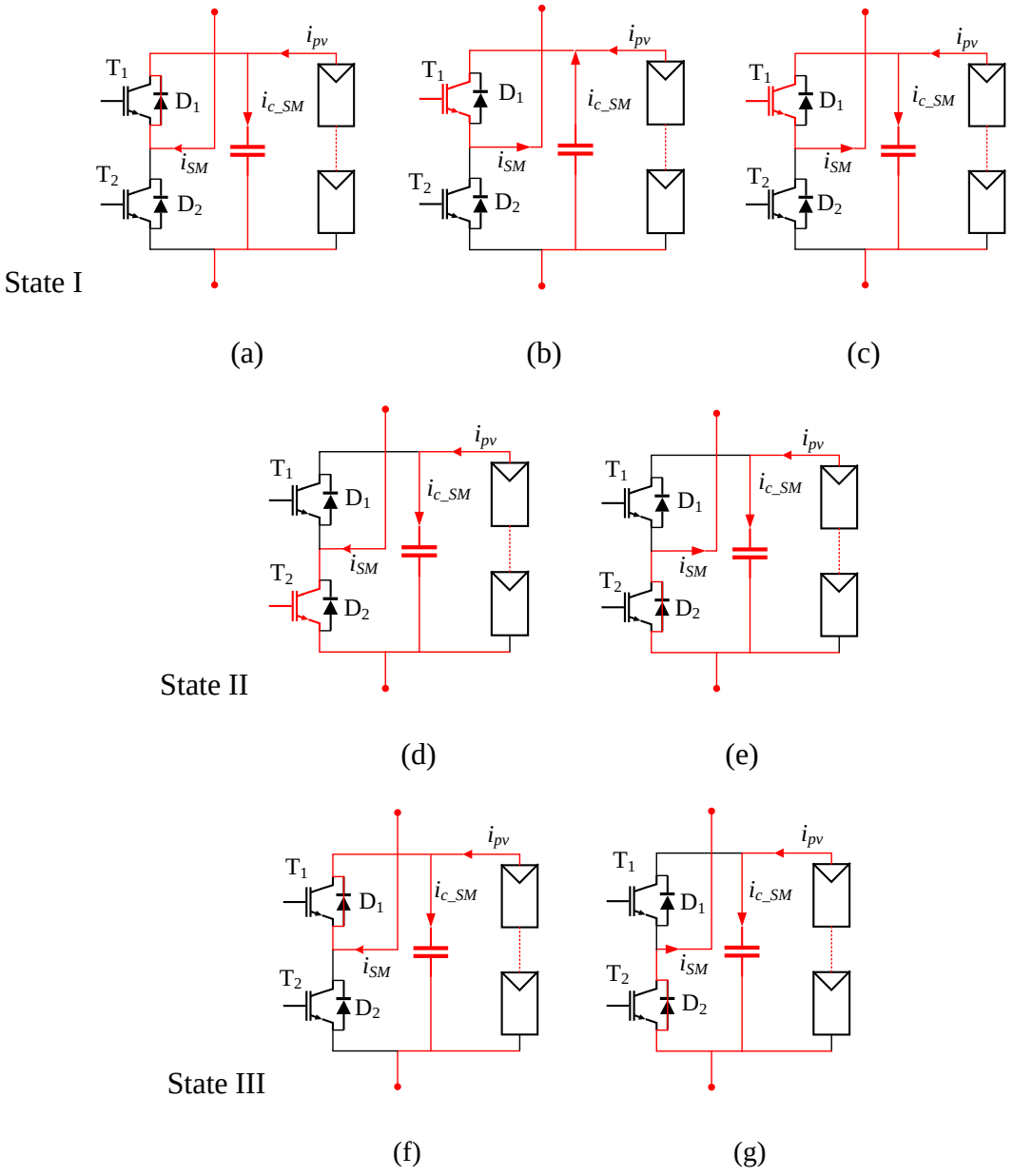

Fig 2.3 Working states of PV – SM.

Besides, the SM voltage equals 0, and the capacitor will be charged by i_{PV}. The ΔU_C is expressed by (7).

$$\Delta U_C = \frac{1}{C}\int i_{PV}\,dt \tag{7}$$

State III: T1 and T2 are switched OFF, and the SM voltage is uncertain. If the SM current flow as shown in Fig 2.3 (f), the capacitor will be charged by i_{SM} and i_{PV} as well as the

Fig 2.3 (a) state. Similarly, the state in Fig 2.3 (g) and Fig 2.3 (e) are the same, the capacitor will be charged by i_{PV}. The ΔU_C is expressed by (8).

$$\Delta U_C = \begin{cases} \frac{1}{C}\int -i_{SM} + i_{PV}\ dt \\ \frac{1}{C}\int i_{PV} dt \end{cases} \tag{8}$$

Both T_1 and T_2 must never be ON state at the same time because a short circuit happens in that situation.

Unlike PV arrays, besides energy harvesting from solar energy, the BESS could be operated under two cases of working states – charging and discharging modes. Therefore, depending on the system control strategy of energy, BESS – SMs could be controlled by some ways. Following this thesis's strategy, the BESSs are approached to be the SM capacitors, respectively. Fig 2.4 shows the BESS – SMs' working states.

According to the description in Fig 2.4, the BESS- SM has two main states including:

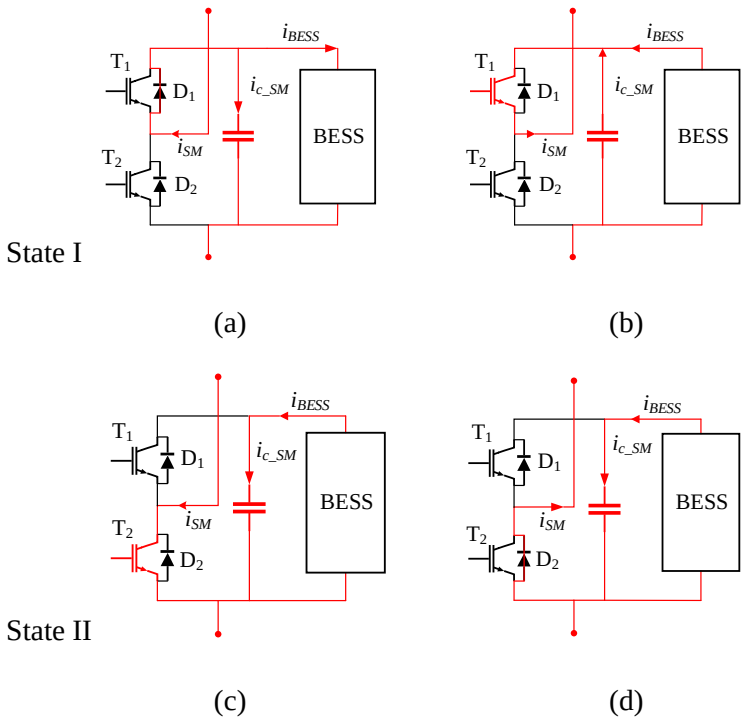

Fig 2.4 Working states of BESS – SMs.

State I: T_1 is switched ON and T_2 is switched OFF. If SM current flows into the SM as shown in Fig 2.4 (a), the i_{SM} will charge to the capacitor and BESS through anti-parallel diode D_1. Vice versa, if the SM current flows out of the SM as shown in Fig 2.4 (b), the capacitor and BESS will be discharged through T_1.

State II: T_1 is switched OFF and T_2 is switched ON. If the SM current flows into the SM as shown in Fig 2.4 (c), the i_{SM} will pass through the T_2. Vice versa, i_{SM} will pass through D_2, if the SM current flows out of the SM as shown in Fig 2.4 (d).

Similarly, switches T_1 and T_2 must never be switched ON at the same time because of a short circuit by capacitor voltage.

2.4. Design of the system

2.4.1. Design of the arm inductor.

In the MMC system, the arm inductor is connected in series with SMs in each arm. The inductors are attacked in MMC to compensate for the different voltage between the total voltage of SM capacitors in the phase and the DC-link voltage. Besides, one of the losses in MMC is circulating currents and they are caused by the different voltages between phase units in the system. Therefore, arm inductance is an important factor to improve the loss and fault currents.

In the MMC system, it is appeared by the resonant frequency ω_{rn}, which is the fundamental frequency for which, the amplitude of the *n*-th harmonic is dependent on the resistance. Besides, the additional resistor could cause losses. Instead of attaching the resistor to avoid that harmonic, adjusting the values of capacitors and arm inductors is possible for the same purpose [28]. The relationship between capacitance and inductance is given in (9)

$$L_{arm}C_{SM} > \frac{5N}{24\omega^2} \tag{9}$$

Where ω is the fundamental angle frequency in radians per second.

The circulating current decreasing is the main purpose for the additional inductor in each arm. In [29], the parameter of the arm inductor at a given circulating current peak value is determined as (10).

$$L_{arm} = \frac{1}{8\omega^2 . C . U_{C\_SM}} . \left(\frac{S}{3I_{cir}} + U_{DC} \right) \tag{10}$$

Where I_{cir} is the desired peak circulating current;

S is the apparent power;

U_{C_SM} is the desired value, which is decided by the number of SMs per arm and gets the value as given as (11).

$$U^*_{C\_SM} = \frac{U_{DC}}{N} \tag{11}$$

2.4.2. Design of the submodule capacitor

Besides neglecting the effect of the circulating current, keeping the stable voltage for SMs is necessary. Because any ripple voltage at the SM capacitor causes poor MPPT at the PV array in PV – SM. Thus, the capacitance C_{SM} needs to be estimated for minimum ripple to avoid poor MPPT, the PV array could be run at the Maximum Power Point (MPP) voltage as possible.

To determine the SM capacitance, the energy in each arm needs to be calculated and divided into the number of SMs per arm. Equation (12) expresses the arm energy.

$$W_{arm} = \frac{2S}{3m_v\omega} \left[1 - \left(\frac{m_v \cos\varphi}{2} \right)^2 \right]^{3/2} \tag{12}$$

where m_v denotes the modulation index and is defined by (13). φ is the corresponding phase angle.

$$m_v = \frac{2\sqrt{2}U_{RMS}}{U_{DC}} \tag{13}$$

with U_{RMS} is the RMS value of output voltage.

As mentioned above, if each arm of the system has *N* SMs, the storage energy in each arm W_{SM} is assigned to N SMs, it is expressed by (14).

$$W_{SM} = \frac{2S}{3Nm_v\omega}\left[1-\left(\frac{m_v\cos\varphi}{2}\right)^2\right]^{3/2} \tag{14}$$

During the working period, the capacitor is charged and discharged depending on working states as in the previous section. Thus, the SM capacitor voltages consist of the ripple arrow the desired value by a range of $\pm\varepsilon$. The following relation could be achieved as (15).

$$U_{C\_SM}(1-\varepsilon) \le U_{C\_SM} \le U_{C\_SM}(1+\varepsilon) \tag{15}$$

The energy of the SM capacitor is given by (16)

$$W_{C\_SM} = \frac{1}{2}CU_{C\_SM}^2 \tag{16}$$

Combining between (14) and (16), the relation is expressed by (17).

$$\begin{aligned} &W_{C\_SM} = \frac{1}{4\varepsilon}W_{SM} \\ &\Leftrightarrow \frac{1}{2}CU_{C\_SM}^2 = \frac{1}{4\varepsilon}\cdot\frac{2S}{3Nm_v\omega}\left[1-\left(\frac{m_v\cos\varphi}{2}\right)^2\right]^{3/2} \end{aligned} \tag{17}$$

Following (17), the SM capacitance could be calculated as (18).

$$C = \frac{S}{3Nm_v\varepsilon\omega U_{C\_SM}^2}\left[1-\left(\frac{m_v\cos\varphi}{2}\right)^2\right]^{3/2} \tag{18}$$

Equation (18) is used to choose the SM capacitance depending on the ripple range of capacitor voltage ε. Typically, ε is selected about 5% of the average capacitor voltage.

2.4.3. Design of BESS

As mentioned early in the thesis, the proposed topology is the hybrid system consists PV arrays and BESSs based on MMC structure. Following that, BESSs run with the role which is compensators for voltage and power per arm. Therefore, it supports reducing the arm power mismatching and circulating currents that lead to decreased losses and keeps stability.

As topology in Fig 2.1 (a), BESS consists of batteries and DC/DC converter, it interfaced to SM at SM's DC side. Therefore, BESSs are designed with a rated power that equals the rated power of SM. Moreover, the number of BESSs based on the total BESS power designed. For smooth operation function, the exchanging BESSs power needs to be suitable to eliminate different power between arms under partial shading and fluctuation power under uneven irradiation conditions. Besides calculating BESSs power, BESS capacity is an important factor needs to be considered to design the system parameters.

The capacity fade rate of the battery is the value reflected in the loss of battery capacity after the working cycle. Thus, it is an important factor to estimate the long life of BESS, it leads effectively to operating, replacing, and profitability with the inventors. The battery's capacity fade based on the influence of cycling time (t), temperature (T), Deep of discharge (DoD), and discharge rate ($Rate$) as illustrated by (19) [30].

$$Q_{loss} = f\ t,T,DoD,Rate \tag{19}$$

Following the thesis limitation, this thesis designs the control scheme and operating analysis of the MMC – based PV and BESS system, so the temperature condition is ignored. As a result, the discharge rate is the main factor influences the battery capacity to fade negatively, the discharge rate is larger which leads to an increase in the aging of battery cells. To ensure working ability and battery life, the discharge rate needs to keep under 1C during all working conditions, which means that the discharge current (kA) needs to keep under 1 time to C (kWh) (C is the capacity of the battery). In the proposed system, due to an array of batteries being connected to SM through a DC/DC converter, therefore the capacity of each BESS (kWh) needs to be at least equal to SM current (kA). Besides discharge rate, the *DoD* is the factor with a smaller effect. The battery life is reduced if the *DoD* gets larger. Figure 2.5 express the relationship between the battery life cycle and the *DoD* decay of a lithium nickel manganese cobalt oxide (NMC) battery [31].

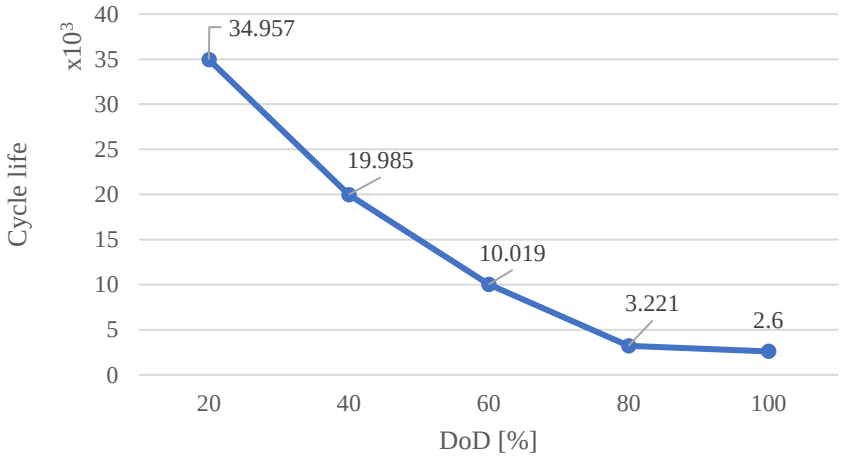

Fig 2.5 Battery Cycle Life as a function of *DoD*

To avoid the effect of *DoD*, 20% *SoC* is considered for the low limit boundary for battery and full *SoC* limitations are given by (20).

$$20\% \le SoC_t \le 100\% \tag{20}$$

Where SoC_t is *SoC* at time *t* and is expressed by (21).

$$SoC_t = SoC_{t-1} + \frac{P_{BESS\_t}.\Delta t}{E_{BESS}}.100\% \tag{21}$$

With SoC_{t-1} is State of Charge at the initial time; P_{BESS_t} is the charged/discharged power, it gets positive if BESS is charged, meanwhile it gets negative when BESS is discharged. E_{BESS} is the battery's energy and Δt presented the time interval.

Besides the Discharge rate condition previously mentioned, the working conditions as well as *DoD* fluctuations during the working time which is one of the factors fade State of Health (*SoH*) of the battery. To estimate the life cycle of the battery for the working conditions, the Rainflow is applied for the BESS system that supports PV plants [32-35]. The Rainflow processing is conducted step by step as below.

Step 1: Use the *DoD* datasheet from history data (or simulation) to make new *DoD* data (DoD_r) by ignoring points between raising and falling periods and keeping the margins for each period.

Step 2: Based on the series of DoD_r points from the first step, the R_x and R_y values are two ranges of the first three points of DoD_r. R_x and R_y are given by (22).

$$\begin{aligned} R_x(t_i) &= \left| DoD_r(t_i) - DoD_r(t_{i+1}) \right| \\ R_y(t_i) &= \left| DoD_r(t_{i+1}) - DoD_r(t_{i+2}) \right| \end{aligned} \tag{22}$$

where t_{i+1}, and t_{i+2} are two points of time after the t_i point in the DoD_r datasheet.

Step 3: The Rainflow cycle (RF) is determined as a full cycle (1) or half cycle (0.5) by following the conditions by (23).

$$RF\ \ t_i = \begin{cases} 0.5, \text{ if } \quad R_x(t_i) < R_y(t_i) \ \text{ and } \ t_i = 1 \\ 1.0, \text{ if } \quad R_x(t_i) < R_y(t_i) \end{cases} \tag{23}$$

Step 4: Repeat from step 1 to step 3 by the next points until all points are calculated.

Following the Rainflow calculated processing above, the Rainflow degradation for the annual datasheet is given by (24)

$$D_{RF}(t_i) = \sum_{i=1}^{n} \frac{RF(t_i)}{A.(DoD)^B} \times 100\% \tag{24}$$

where D_{RF} is the rainflow degradation, A and B are empirical parameters of battery specifications.

Besides the Rainflow algorithm being applied for the significant changing of DoD, the calendar degradation is applied additionally for light contributions (in a light sunny day or light fluctuations of irradiation). In these conditions, the batteries still work with small degradation, it is estimated about 3 % loss of battery capacity per year [32-36]. And daily degradation based on calendar degradation is given by (25)

$$D_{calendar}(t) = \frac{3\% / year}{365.25 days / year} = 0.008\%\ loss / day \tag{25}$$

where $D_{calenadar}(t)$ is daily degradation, the total annual degradation of BESS is the sum of the calendar degradation and the rainflow degradation as expressed in (26).

$$D_{TL} = \sum D_{DF} + \sum D_{calendar} \tag{26}$$

where D_{TL} is the total annual degradation of BESS. The estimated BESS capacity needs to satisfy two conditions – the discharge rate is under 1C and D_{TL} is under the BESS life target. If it is not satisfying, the 5% increase in BESS capacity is considered and conducted rainflow processing until (26) satisfied.

Chapter 3. Control of the hybrid MMC – based PV and BESS

This thesis proposed the hybrid MMC – based PV and BESS system. Taking advantage of the conventional method, grid-connected control and individual capacitor voltage control has remained. To adopt working conditions by BESS contribution under uneven irradiances, the control method is released, which consists of three main control: grid-connected control, individual capacitor voltage control, and BESS control.

3.1. Grid-connected control

The grid-connected control depends on the current control. According to the single-phase equivalent circuit of the system in Fig 2.2, the AC output voltage of the system u_u is expressed by (27).

$$u_{t\_u} = -Ri_u - L\frac{di_u}{dt} + u_u \tag{27}$$

when *R* and *L* are the resistors and the inductor of the system, subscript *u* of voltage and current denotes for each phase (*u* = *a*, *b*, *c*) By using the *abc/dq* transformation, the AC output voltage could be rewritten in the *dq*-frame as (28)

$$\begin{aligned} u_{td} &= -Ri_d - L\frac{di_u}{dt} + u_{sd} + \omega Li_q \\ u_{tq} &= -Ri_q - L\frac{di_q}{dt} + u_{sq} - \omega Li_d \end{aligned} \tag{28}$$

where u_{td}, u_{tq}, u_{sd}, u_{sq}, i_d and i_q denote the *dq*-axis components of voltages and current of the system, respectively. According to the relationship in (28), the AC output voltage is regulated by the current. Through the combination of the PI controller, (28) is expressed as (29).

$$\begin{aligned} u_{td}^{*} &= -(K_1 + \frac{K_2}{s})(i_d^{*} - i_d) + u_{sd} + \omega Li_q \\ u_{tq}^{*} &= -(K_1 + \frac{K_2}{s})(i_q^{*} - i_q) + u_{sq} - \omega Li_d \end{aligned} \tag{29}$$

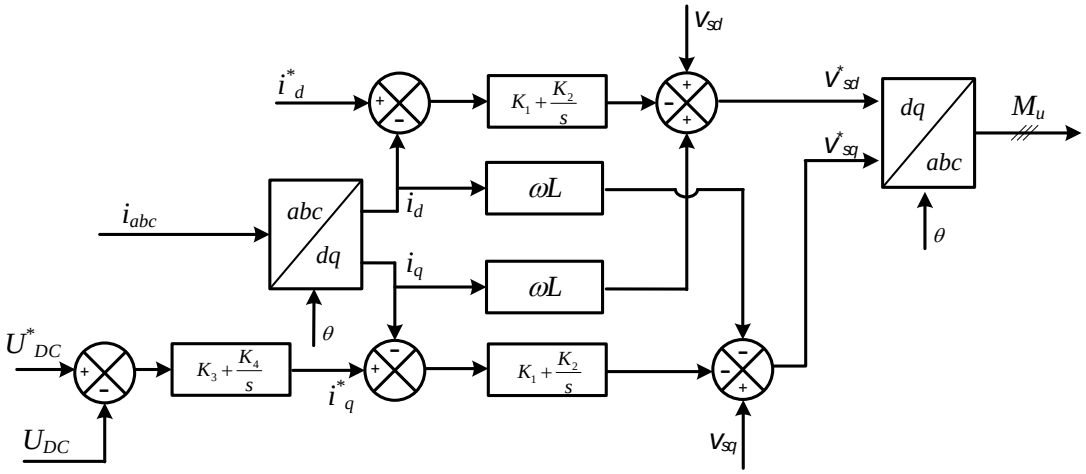

Fig 3. 1 The overall grid-connected control of the MMC – based PV and BESS system.

when superscript * presents the reference value.

Besides supporting the estimated values of i_d^* and i_q^* for the current control, using a DC-link voltage-loop control is one of the common methods to regulate the *d/q* axis component of the current reference [15, 16, 18, 24, 37] as well as i_q^* in this thesis. To maintain the constant DC-link voltage, the PI controller is applied, and the i_q^* signal is defined through the result after the DC-link voltage loop control, it is given by (30). The reference of the *d*-axis component of current is set $i_d^* = 0$ as well as keeping output reactive power equal to 0. The overall grid-connected control is illustrated in Fig 3.1.

$$i_q^* = (K_3 + \frac{K_4}{s})(U_{DC}^* - U_{DC}) \tag{30}$$

3.2. PV – SM capacitor voltage balancing

In the MMC system, the balancing of SM capacitor voltage keeps an important role. That ensures balancing about arm voltage between arms, therefor it makes smaller circulating currents. So the loss is decreased by the circulating current decreasing [38]. Moreover, the failure in SM voltage balancing makes more fluctuation in capacitor voltage not only distorting the output voltage but also decreasing life or damaging equipment.

By necessary of capacitor voltage balancing in MMC, some algorithms are released to support this function, there are two main algorithms as sorting method [39-42] and individual capacitor voltage balancing [43-46]. Both methods approach a minimum ripple compared between capacitor voltage and the desired voltage. The sorting method approaches the balance by controlling the ON/OFF state of switches that control capacitor charge/discharge. By that, the capacitor voltage gets a small ripple without the exact desired value. Unlike the sorting method, the individual capacitor voltage balancing achieves the balance depending on the exact referent value of the capacitor voltage. Therefore, the individual capacitor voltage balancing is suitable for the conventional and proposed methods because the MPPT could be applied without a DC/DC converter. Thus, the PV array could work at the MPP voltage, so each PV – SM could be harvested the maximum power from their PV array.

The individual SM capacitor voltage balancing could be divided into two parts:

PV – SMs leg average voltage control.

The individual voltage control.

3.2.1. PV – SMs leg average voltage control

To keep the balance voltage between PS – SMs in the legs, by that the circulating current between phases. Fig 3.2 (a) shows the PV – SMs leg average voltage control in detail. The control consists of two loop controls – voltage and current loop of control. The reference to the voltage loop is the average of all MPPT voltages of PV arrays ($\overline{U}_{MPPT}$) in the leg, it is given by (31). Which is compared to the average of all voltages of PV arrays ($\overline{U}_{PV}$) in the leg, it is expressed by (32)

$$\overline{U}_{MPPT} = \frac{1}{k}\sum_{j=1}^{k} U_{MPPT\_j} \tag{31}$$

$$\overline{U}_{PV} = \frac{1}{k}\sum_{j=1}^{k} U_{PV\_j} \tag{32}$$

where U_{MPPT_j} is the MPPT voltage of the PV array and U_{PV_j} is the PV array voltage at *j*-position in the leg with *k* is the number of PV – SMs in the leg.

According to the control in Fig 3.2, the circulating current reference is defined as (33), then it is compared to the circulating current in the current loop control to get the control voltage value, u^*_{ref1} given by (34).

$$i^*_{cir\_u} = (K_5 + \frac{K_6}{s})(U_{MPPT\_u} - U_{PV\_u}) \tag{33}$$

$$u^*_{ref1\_u} = (K_7 + \frac{K_8}{s})(i_{cir\_u} - i^*_{cir\_u}) \tag{34}$$

with the circulating current given by (1).

3.2.2. Individual voltage control

Individual capacitor voltage balancing [47] is considered in this thesis to take the role, which approaches MPPT for each PV array in the proposed system. Fig 3.2 (b) shows a block diagram of the individual capacitor voltage for PV – SMs in the system to achieve their MPPT, the voltage control for BESS – SM is presented in the next section. As working states are given in section 2.2, the PV – SM capacitor voltage as well as the PV array voltage is influenced by the arm current direction in which they are. Therefore, the result of individual PV – SM capacitor voltage, $u^*_{ref2\_uj}$ get a positive error of comparison between individual MPPT voltage and the PV array voltage if their arm current is positive. Versa if the arm current is negative, $u^*_{ref2\_uj}$ get negative of the voltage comparing error. Finally, $u^*_{ref2\_j}$ is represented by (35).

$$u^*_{ref2\_uj} = \begin{cases} K_9(U_{MPPT\_uj} - U_{PV\_uj}) & (\text{if } i_{up\_u}, i_{low\_u} > 0) \\ -K_9(U_{MPPT\_uj} - U_{PV\_uj}) & (\text{if } i_{up\_u}, i_{low\_u} < 0) \end{cases} \tag{35}$$

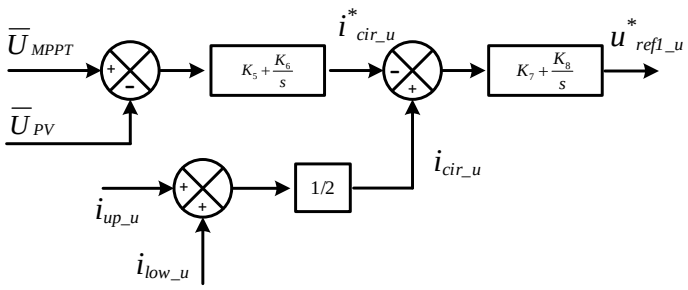

(a)

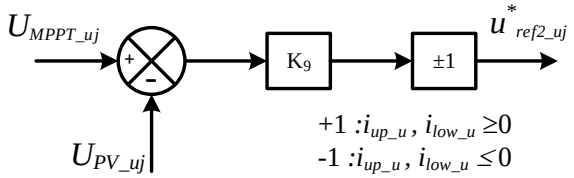

(b)

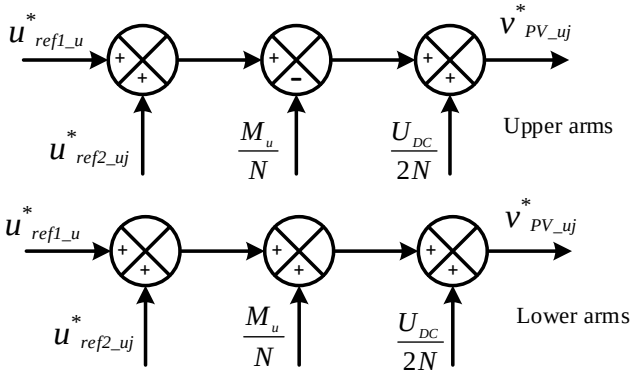

(c)

Fig 3.2 The individual PV – SM capacitor voltage balancing algorithms: (a) The PV – SMs leg average voltage control; (b) The individual voltage control; (c) Final PV – SMs control references

In the conventional method, (35) is applied for redundancy SM voltage control with reference is essential compensated voltage for their arm. The final PV – SMs control references are given by (36) for both the upper and lower arm, respectively.

$$\begin{aligned} u^*_{PV\_uj} &= u^*_{ref1\_u} + u^*_{ref2\_uj} - \frac{M_u}{N} + \frac{U_{DC}}{2N} \quad \text{(upper arm)} \\ u^*_{PV\_uj} &= u^*_{ref1\_u} + u^*_{ref2\_uj} + \frac{M_u}{N} + \frac{U_{DC}}{2N} \quad \text{(lower arm)} \end{aligned} \tag{36}$$

where $u^{*}_{PV\_uj}$ is the final PV – SMs control reference at the *u*-phase and *j*-position. Then, they are compared with triangle waves following phase-shift modulation for MMC [43].

3.3. BESS control scheme

As early mentioned in the thesis, the BESSs are embedded arms of the hybrid MMC – based PV to adapt two main functions as well as eliminating power output fluctuations and arm power mismatching under partial shading of illumination besides compensation of arm voltages.

In the conventional system, it includes a redundant SM as a voltage compensator for each arm. Therefore, the arm voltages are kept balancing under variation working conditions. Meanwhile, the proposed system consists of BESSs with a power compensating function instead of voltage compensating only. Unlike the conventional system, BESSs could be regulated voltage early through DC/DC converter. The voltage referent value for each arm depended on the voltage needed to compensate for each arm like the conventional method, which is expressed by (37)

$$U^{*}_{BESS\_k} = \frac{1}{x}\left(U^{*}_{DC} - \sum_{j=1}^{N} U_{PV\_j} \right) \tag{37}$$

where $U^{*}_{BESS\_k}$ the voltage reference for the DC/DC converter of BESS, means BESS voltage reference.; *x* is the number of BESS – SM in each arm.

To adapt the power compensating function, BESS control consists of power smooth control and arm power mismatching control for their functions, respectively.

3.3.1. Smooth power control

Due to the natural fluctuation of irradiation, it makes the ripple of power output during the working time. As this reason, BESSs are embedded in the proposed system. For that, to get smoothly at the power output, the Moving Average Filter (MAF) is the method with the most

common application [25, 48, 49]. The moving average filter is a smoothing method that provides an average value of input data within a window size, the output of the filter gets smoother if the window size is larger, and the MAF mathematical that is applied in the proposed system is described as by (38).

$$P_{MAF}(t) = \frac{1}{m}\sum_{i=1}^{m} P_{O\_i} \tag{38}$$

where $P_{MAF}(t)$ is the power output after MAF, m is the number of samples during the window size, P_{O_i} is the power point in the window size.

Due to the irradiation fluctuation happening in all arms at the same time. Therefore, the exchanging power from BESSs is divided into all of BESSs so each BESS compensates with the same value for all BESSs in the system, and is described as (39).

$$P_{BESS}^{MAF} = K_{10}.\frac{P_{MAF}(t) - P_O(t)}{6} \tag{39}$$

where P_{BESS}^{MAF} is one of the power references of each BESS. Sine exchanging power from P_{BESS}^{MAF} reference supports for eliminating output power fluctuation only, so it has no effect to reduce arm power mismatching by partial shading of irradiation.

3.3.2. Power mismatching elimination

One popular condition that happens in PV plants with large scale, is partial shading of illumination. Similarly, the irradiation illuminates to PV – SMs in each arm is different from that, power from each arm is different, it is called by arm power mismatching in the MMC – based PV system. Thus, to eliminate the arm power mismatching, this thesis proposed the hybrid MMC – based PV and BESS.

To adapt to their function, the arm average power control is conducted power balancing for all of the arms in the system. For that, the average power between arms is the reference for the control, it is given as (40). By the control, the BESSs' contribution leads to getting a small

power difference. Therefore, if the arm power is smaller than the average power, BESSs in the arm will discharge. Versa, BESSs will charge if their arm power is larger than the average power, respectively. The arm average power control is expressed for each BESS as (41)

$$P_{arm\_avg} = \frac{1}{6}\sum_{n=1}^{6} P_{arm\_n} \tag{40}$$

$$P_{BESS\_k}^{AVG} = \frac{1}{x}(K_{11} + \frac{K_{12}}{s})(P_{arm\_avg} - P_{arm\_n}) \tag{41}$$

where P_{arm_avg} is the arm average power of the system, P_{arm_n} is the *n*-th arm power. $P_{BESS\_k}^{AVG}$ is the power reference of each BESS in the *k*-th arm with *x* of the number BESS in the arm.

The combination of two functions of power smooth and arm power mismatching elimination, the final power reference for each BESS in the system is expressed by (42).

$$\begin{aligned} P_{BESS\_k}^{*} &= u_{ref1}^{*} + (P_{BESS}^{MAF} + P_{BESS\_k}^{AVG})\left(-\frac{M_u}{N}\right) + \frac{U_{DC}}{2N} \text{ (upper arm)} \\ P_{BESS\_k}^{*} &= u_{ref1}^{*} + (P_{BESS}^{MAF} + P_{BESS\_k}^{AVG})\left(\frac{M_u}{N}\right) + \frac{U_{DC}}{2N} \text{ (lower arm)} \end{aligned} \tag{42}$$

where $P_{BESS\_k}^{*}$ is the final power reference for each BESS. Then, $P_{BESS\_k}^{*}$ is compared to triangle ways according to their phase-shift similar $u_{PV\_uj}^{*}$ references of PV – SMs.

Chapter 4. Simulation Results

To ensure the BESSs' contribution and operation stability of the proposed system, the simulations are conducted in PSCAD software under variation working conditions of irradiation fluctuation and partial shading as mentioned. Besides, the contribution of the proposed system is presented by comparing the operation between the proposed system and the conventional one in the same studied cases.

In this thesis, the proposed method is applied in the hybrid MMC – based PV and BESS 10 MW, 11-level (N=10) with 8 PV – SMs and 2 BESS – SMs per arm. And the conventional one is a hybrid MMC – based PV system 12 MW, 11-level with 9 PV – SMs and a redundant SM (the SM without BESS). Both system structures are presented in Fig 4. 1 with the parameters listed in Table 4. 1. Moreover, the PV array parameters are attached in Table 4. 2.

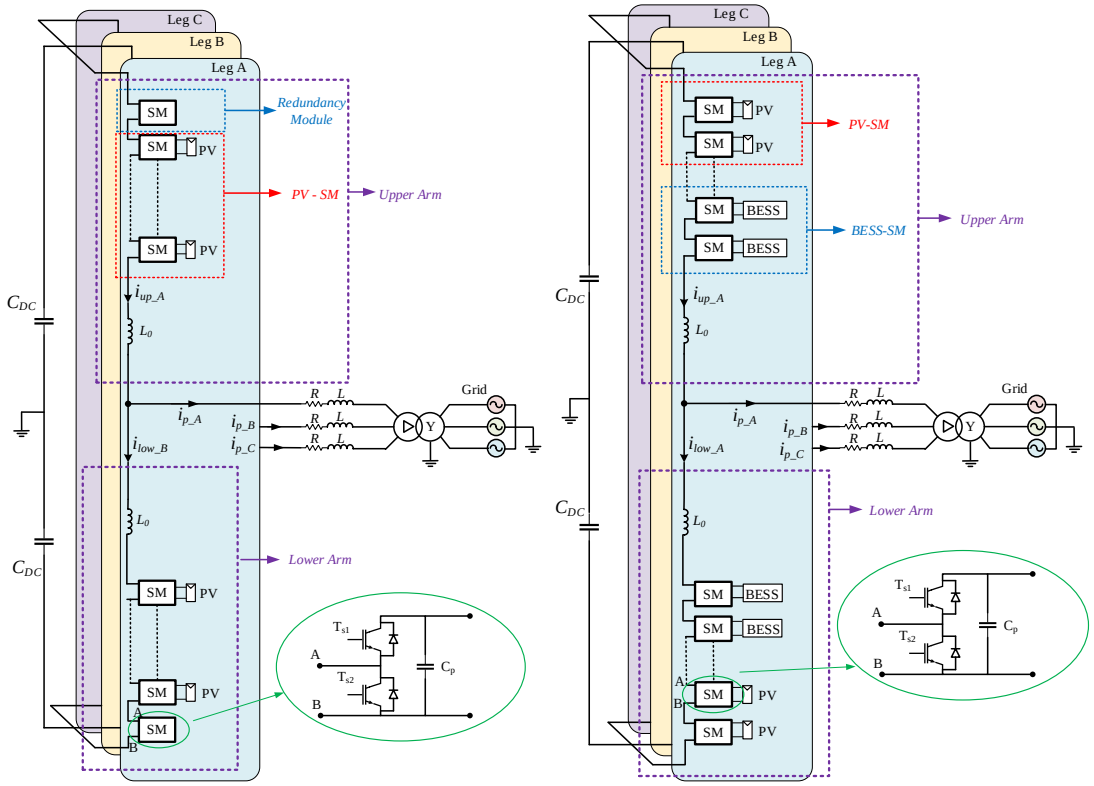

(a) (b)

Fig 4. 1 The simulation systems; (a) The conventional structure; (b) The proposed structure.

Table 4. 1 The MMC system parameters

Parameter	Value	Units
Maximum Power	10	MW
DC voltage	9	kV
Arm inductance L	2	mH
Arm resistance R	0.01	Ω
Filter inductance	1	mH
SM capacitor C	20	mF
DC bus capacitor C_{DC}	10	mF
The number of SMs per arm	10	-

Table 4. 2 The PV – SM parameters

Parameters	Value (Proposal/Conventional)	Units
Rated PV-SM power	0.18/0.16	MW
Number of series PV	37/37	-
Number of parallel PV	90/80	-
PV arrays short-circuit current I_{sc}	0.2263/0.2012	kA
PV arrays open-circuit voltage V_{oc}	1.11	kV

And controller parameters are presented in Table 4. 3.

4.1. The power smoothly

In this case, the changing irradiation is the condition to conduct the simulations. The irradiation data are collected by [50]. To reduce the simulation time, the time resolution from collected data is scaled by 153.6 times, which means 20 s in the simulation concerning3072 s in reality, and the window size is 1 s for 153.6 s in reality, respectively.

Table 4. 3 The Controller parameter

Parameters	Value	Parameter	Value
K_1	5	K_7	1
K_2	1000	K_8	10
K_3	1	K_9	1
K_4	10	K_{10}	6
K_5	2	K_{11}	5
K_6	10	K_{12}	100

The irradiation data are presented in Fig 4.2 (a). According to the figure, the irradiating has fluctuation during the working time, at t = 9.7 s the irradiation (I_m) gets a minimum value of about 430 W/m^2, and a maximum of about I_m = 985 W/m^2 at t = 15.6 s.

As the results of output power are presented in Fig 4.2 (b), the conventional system reaches the maximum power of about 8.43 MW at t = 9.3 s and when I_m = 970 W/m^2, and a minimum of about 3.75 MW at t = 9.7 s before the ramp up (ramping up at t > 9.7 s) that caused lost control for the conventional method. For the proposed system, although the rated power of all PV arrays is the same as the conventional one, it only reached 7.7 MW at t = 9.7 s by it charged BESSs to decrease fluctuation in output power. Similarly, BESSs discharged, which leads to reduce ripple output when it reached 4.78 MW at t = 9.7s instead of 3.75 MW from the conventional system. During that period, the proposed system shows it achieved output power more smoothly than the conventional one. And that is the evidence to prove the contribution of BESSs and their control with MAF is the main function in this scenario.

During all simulation times of the proposed system, the maximum power reaches 8.05 MW at t = 15.6 s and 4.78 MW at t = 9.7 s, when Im gets the maximum and minimum values, respectively. For that, BESS exchanging power is shown in Fig 4.2 (c), the BESSs discharged when output power suddenly decreased and charged when output power increased, respectively. As a result, the BESSs get a maximum discharging of about 1.67 MW at t = 2.7

s and maximum charging of about 0.8 MW in the periods from t = 8.5 s to 9.3 s and from t = 12.6 s to t = 14.1 s. Thus, the exchanging power from BESSs gets more ripple when the output power gets more ripple also.

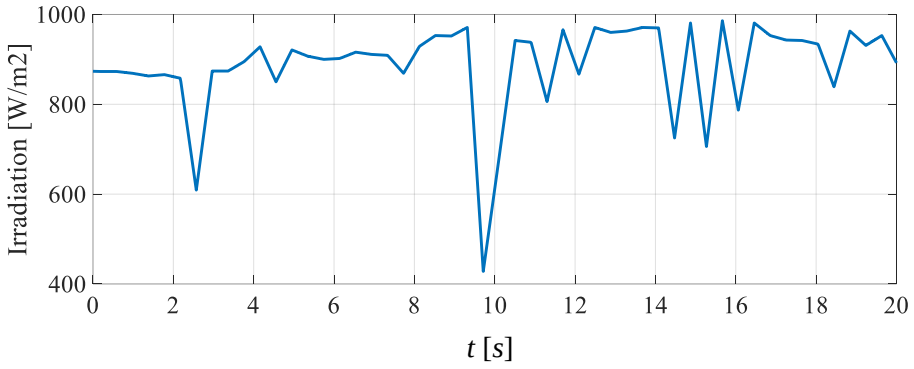

(a)

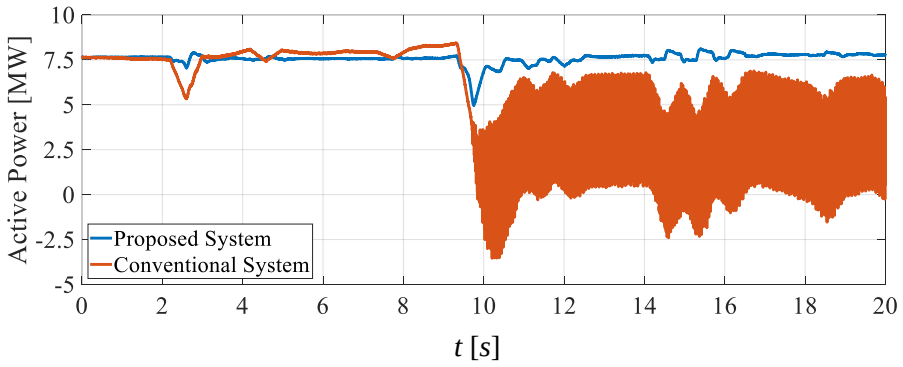

(b)

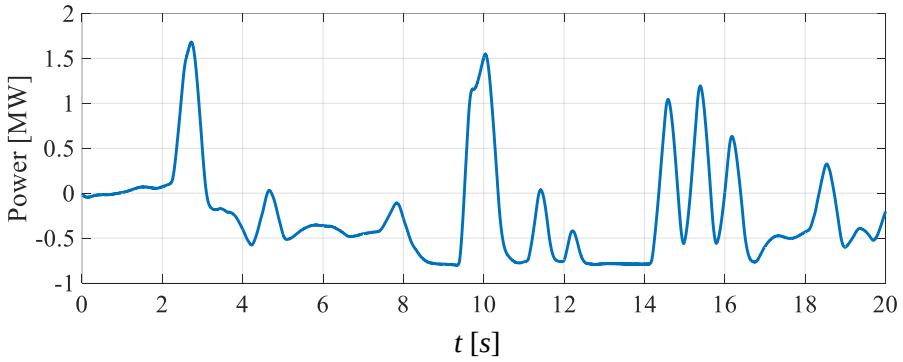

(c)

Fig 4.2 The irradiation data and output power of both systems in the fluctuation of irradiation condition; (a) the irradiation condition; (b) the power of both systems; (c) the total exchanging power from BESSs.

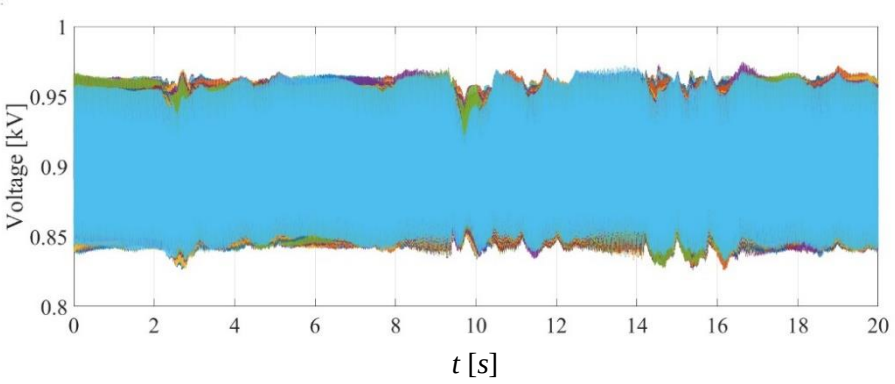

Fig 4.3 The SM voltages of the proposed system

One of the factors to evaluate the MMC system is the SM voltage balancing. According to Fig 4.3, the proposed system shows their balancing at the SM voltage ripple, the ripple gets larger or smaller based on the output power getting larger or smaller, respectively as shown in Fig 4.2.

Additionally, the THD standard is an important factor for grid-connected converters and 5 % THD of voltage from IEEE [29] is the most common standard for the converters that are accepted to connect to the grid. As a result, Fig 4.4 shows the THD of both systems, the conventional system operated under 3 % for a small ramp of irradiation as it is from t = 0 s to 9.7 s as shown in Fig 4.4 (a). Because of the big ramp up after t = 9.7 s, the conventional system is fallen down so the THD gets so high and lost work. Besides, the THD is proportional to the input irradiation, which means that the output voltage gets more harmonic if the system is illuminated more, and versa it gets low harmonic if it receives low illumination. Meanwhile, in the proposed system, the THD approaches under 5 % during all working time, the main factor effect to the THD is the working states of BESS. Following that, if the BESSs discharge or no power exchange, the output voltage consists of about 2 %, otherwise if the BESSs receive energy to charge, the harmonic will be higher based on the magnitude of charged power as THD is about 4 % when it is charged about 0.8 MW as shown in Fig 4.4 (b).

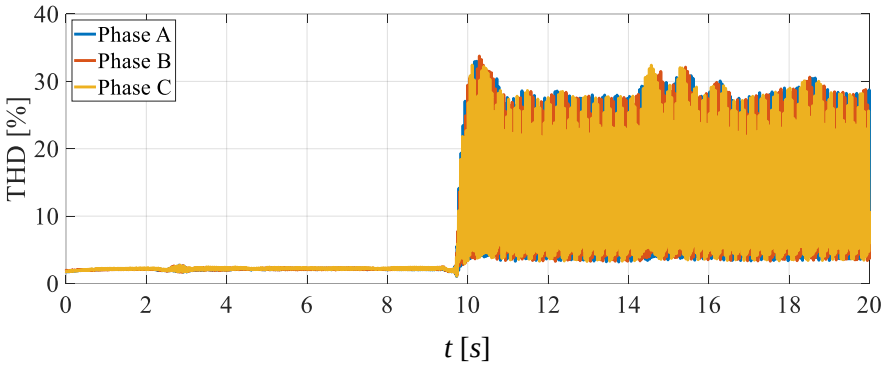

(a)

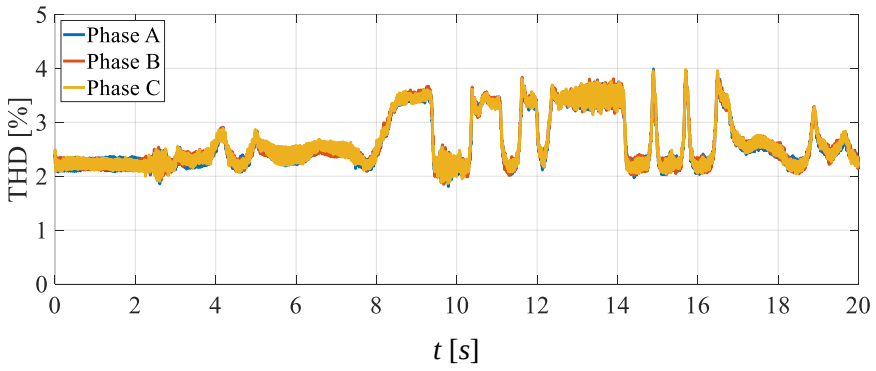

(b)

Fig 4.4 The THD of both systems in the fluctuation of irradiation condition; (a) The THD of the conventional system; (b) The THD of the proposed system

4.2. Arm power mismatching elimination

As the first studied case, this section conducted the operation of both systems in partial shading conditions to perform the power mismatching elimination function. As a part of BESS control, the arm average power is the main function of BESS control to keep a minimum power difference between arms. Besides, MAF is maintained during the operating time, so the power smoothing is kept in this case. Following the partial shading, the irradiation is set as an illustration in Fig 4.5 (a). According to the figure, the 6-*th* arm receives irradiance changing first. Initially, solar irradiance is 800 W/m^2 and keep until 1 s. The irradiance increases from 800 to 1000 W/m2 in t = 1 s to t = 3 s and maintains 1000 W/m^2 in 2 s. From the fifth to the

seventh second, irradiance reduces from 1000 to 600 W/m2 and maintains in 2 s. Then, the irradiance raises to 850 W/m2 from the ninth to the 18th second. For that, the irradiances for arms get delayed 1 s, 2 s, 4 s, 5 s, and 8 s for arms 4, 3, 5, 2, and 1, respectively.

As a result, the output power of both systems is shown in Fig 4.5 (b). Due to the BESS contribution combined with their control, the proposed system could operate for all of the working time with the output power smoothly. It gets maximum power at t = 5.39 s with an output power is 7.63 MW and a minimum of about 5.34 MW at *t* = 12s. But, the conventional system could not work with the same irradiation of conditions for all of the simulation time, it lost control from *t* = 9 s when the irradiations illuminated to arms heterogeneously with the large differences between arms. It happened by the arm power mismatching is so large as shown in Fig 4.6 (a).

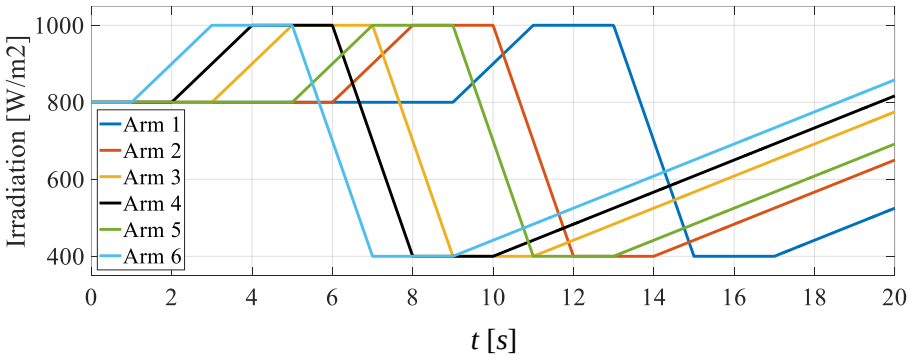

(a)

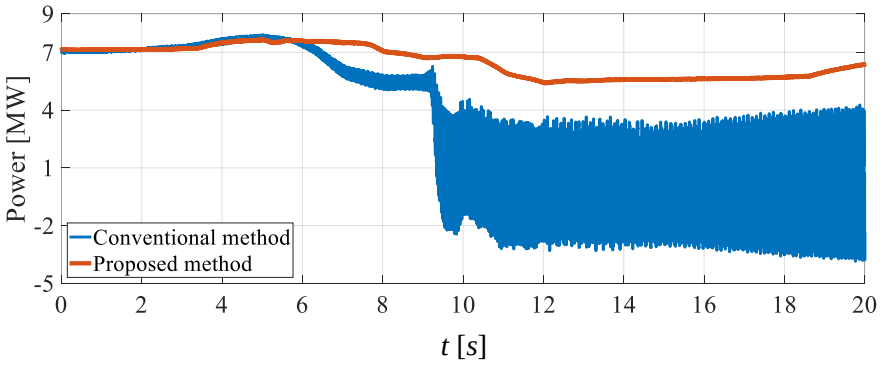

(b)

Fig 4.5 The irradiation data and output power in the partial shading condition; (a) The irradiation data; (b) The output power of both systems

Fig 4.6 (b) shows the arm power of the proposed systems, the proposed one shows their advantages when power from arms approaches the values with small ripples of about 5 % to each other at t = 5.3 s, 9.5 s, and 14 s when the compensated power from BESSs is maximum ability. Therefore it leads to work stability with the small THD.

As a result, the conventional system could not work for all of the simulation time. Therefore, the harmonic gets high when it lost working. But, during its stable time (from t = 0 to t = 8 s), the THD reaches a maximum of 2.5 % which is a strong point for the conventional system compared to the proposed system with 3.35 % under small differences in partial shading of illumination as shown in Fig 4.7 (a). Figure 4.7 (b) presented the stable operation of the proposed system with THD of the output voltage under 3.5 % during the simulation time. The maximum THD of about 3.35 % happened at t = 5.3 s when power from arm 6 gets the ripple.

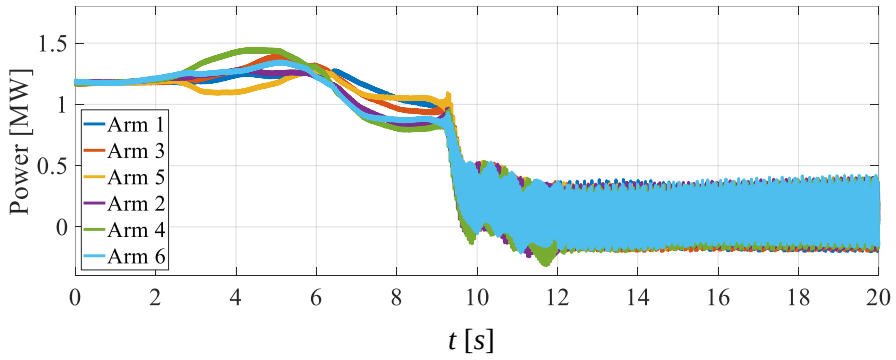

(a)

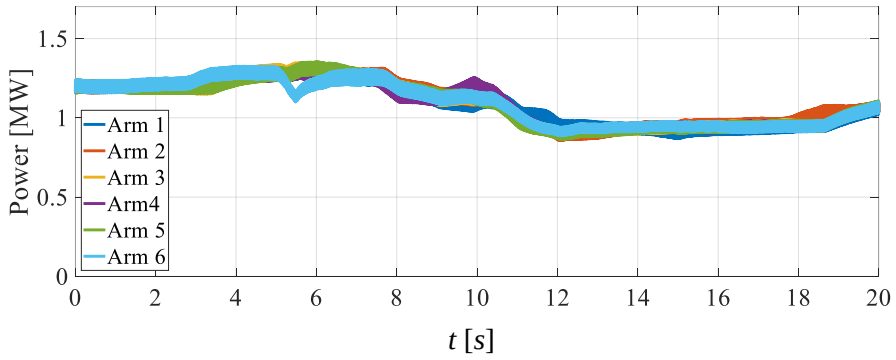

(b)

Fig 4.6 The arm power of both systems; (a) The conventional system; (b) The proposed system

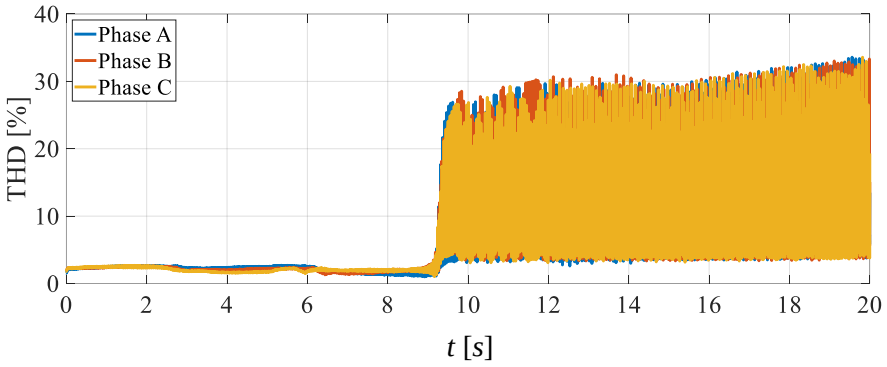

(a)

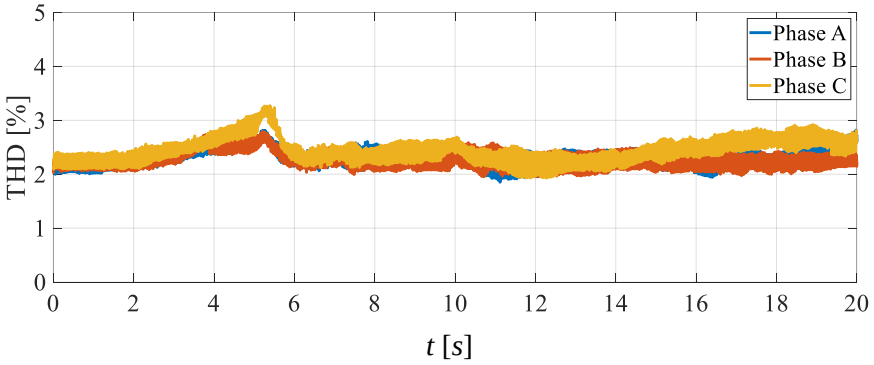

(b)

Fig 4.7 The THD of both systems in partial shading condition; (a) The conventional system; (b) The proposed system

Chapter 5. Conclusion

As the target, this thesis proposed a hybrid MMC – based PV and BESS system successfully with more advantages. Taking the benefits from the conventional system, the proposed system is the solar harvesting system with MMC as the main converter, total PV panels are divided into many arrays that each array connects to MMC at the DC side of SM directly without a DC/DC converter. Therefore, low switching losses by DC/DC converters and low harmonic are strong points that are kept besides handing out poor MPPT distribution. By the complexity of the working conditions, the output power gets the oscillation under fluctuation of irradiation and arm power mismatching under partial shading conditions. Therefore, embedded BESSs are added to arms as the proposed system.

To ensure stable operation, the control method is released, it consists of the grid-connected control to interface with the grid; The individual voltage control to keep PV arrays running with their MPPT voltage so MPPT contribution is achieved; BESS control with power smoothy control to decreased ripple in output power by exchanging power from BESSs, and the arm average power control approach the arm power balancing, it leads to reduce THD in the partial shading conditions.

Besides the topology and control, which are proposed in this thesis, it introduced the methods to estimate the BESS capacity. Following the methods, BESS could be sized for long life target with calendar fade and Rainflow algorithms degradation estimation, and DoD condition to be suitable for the proposed operation.

To prove the operating system, the simulations are conducted in PSCAD software for both, the conventional system and the proposed system. As a result, the proposed system shows good performance under two cases of simulations; In the power smooth scenario, it presented BESSs' role in eliminating power fluctuation by the natural ripple of irradiation conditions, meanwhile, the conventional system got falling when experiencing a large ramp up of

irradiation. Moreover, the proposed system is possible to work stability under partial shading by decreasing power mismatching between arms depending on the BESSs contribution instead of lost work when more difference of irradiation happened. Besides, the proposed system encourages the grid-connected ability by under 5% THD for two common kinds of uneven irradiation.

Aside from the advantages above, this thesis has the weakness of cost feasibility. The modified structure indicates that its operation approach is more stable than the conventional one for both simulation scenarios from BESS contribution so it can support the power system by making the most available resources without degrading the power quality. Meanwhile, the costs incurred for BESS that was not discussed and considered as a factor to compare the impact between the two methods except for technique. From that point of view, the method proposed in this thesis is applied as a "grid-forming" power converter. Additionally, this thesis proposed a control method for the hybrid structure with non-optimization of control parameters so the values of controllers are chosen by tuning P gains and I gains of PI controller. The weak points in this thesis are the motivation for future study.

References

[1] IEA. "Electricity." https://www.iea.org/fuels-and-technologies/electricity (accessed 11/17, 2022).

[2] P. Friedlingstein *et al.*, "Global Carbon Budget 2022," *Earth System Science Data*, vol. 14, no. 11, pp. 4811-4900, 2022, doi: 10.5194/essd-14-4811-2022.

[3] D. M. Scholten, N. Ertugrul, and W. L. Soong, "Micro-inverters in small scale PV systems: A review and future directions," in *2013 Australasian Universities Power Engineering Conference (AUPEC)*, 29 Sept.-3 Oct. 2013 2013, pp. 1-6, doi: 10.1109/AUPEC.2013.6725465.

[4] J. Jana, H. Saha, and K. Das Bhattacharya, "A review of inverter topologies for single-phase grid-connected photovoltaic systems," *Renewable and Sustainable Energy Reviews*, vol. 72, pp. 1256-1270, 2017/05/01/ 2017, doi: 10.1016/j.rser.2016.10.049.

[5] F. Blaabjerg, *Control of Power Electronic Converters and Systems: Volume 3*. Academic Press, 2021.

[6] S. Deshpande and N. R. Bhasme, "A review of topologies of inverter for grid connected PV systems," in *2017 Innovations in Power and Advanced Computing Technologies (i-PACT)*, 21-22 April 2017 2017, pp. 1-6, doi: 10.1109/IPACT.2017.8245191. [Online]. Available: https://ieeexplore.ieee.org/document/8245191/

[7] N. Foureaux, A. Machado, S. É, I. Pires, J. Brito, and F. Braz Cardoso, "Central inverter topology issues in large-scale photovoltaic power plants: Shading and system losses," in *2015 IEEE 42nd Photovoltaic Specialist Conference (PVSC)*, 14-19 June 2015 2015, pp. 1-6, doi: 10.1109/PVSC.2015.7355828.

[8] R. Marquardt, "Stromrichterschaltung mit verteilten Energiespeichern und Verfahren zur Steuerung einer derartigen Stromrichterschaltung," *Patentschrift DE 101 03 031 B4*, 2001.

[9] J. Cao and J. Y. Cai, "HVDC in China," in *2013 HVDC and FACTS Conference, Palo Alto, CA, USA*, 2013.

[10] SIEMENS. "HVDC PLUS: A new approach for new challenges." https://www.siemens-energy.com/global/en/offerings/power-transmission/portfolio/high-voltage-direct-current-transmission-solutions/hvdc-plus.html (accessed 02/03, 2022).

[11] H. Energy. "STATCOM - SVC Light®." https://www.hitachienergy.com/offering/product-and-system/facts/statcom/svc-light (accessed 02/03, 2022).

[12] G. G. Solution. "Static Synchronous Compensator." https://www.gegridsolutions.com/powerd/catalog/statcom.htm (accessed 02/03, 2022).

[13] H. Bayat and A. Yazdani, "A Power Mismatch Elimination Strategy for an MMC-Based Photovoltaic System," *IEEE Transactions on Energy Conversion*, vol. 33, no. 3, pp. 1519-1528, 2018, doi: 10.1109/TEC.2018.2819982.

[14] B. Wang, S. Liu, and X. Wu, "Study on the Control Scheme of Energy Storage MMC," in *2019 IEEE Sustainable Power and Energy Conference (iSPEC)*, 21-23 Nov. 2019 2019, pp. 1990-1996, doi: 10.1109/iSPEC48194.2019.8975282.

[15] S. B. Bashir, H. A. Zidan, and Z. A. Memon, "Power balancing of grid connected PV system based on MMC under different irradiation conditions," *International Journal of Electrical Power & Energy Systems*, vol. 117, p. 105717, 2020/05/01/ 2020, doi: 10.1016/j.ijepes.2019.105717.

[16] S. Barcellona, M. Barresi, S. Colnago, and L. Piegari, "MMC-PV System with dc-link integrated battery energy storage system," in *2021 IEEE 15th International Conference on Compatibility, Power Electronics and Power Engineering (CPE-POWERENG)*, 14-16 July 2021 2021, pp. 1-8, doi: 10.1109/CPE-POWERENG50821.2021.9501215.

[17] J. Khazaei, G. Pavlak, B. Lee, and M. Elsenbaty, "A Novel Application of Modular Multi-Level Converters for Partially Shaded PV Systems," in *2019 IEEE Texas Power and*

Energy Conference (TPEC), 7-8 Feb. 2019 2019, pp. 1-6, doi: 10.1109/TPEC.2019.8662179.

[18] F. Mohamed, S. Wasti, S. Afshar, P. Macedo, and V. Disfani, "MMC-Based Distributed Maximum Power Point Tracking for Photovoltaic Systems," in *2020 IEEE Power & Energy Society General Meeting (PESGM)*, 2-6 Aug. 2020 2020, pp. 1-5, doi: 10.1109/PESGM41954.2020.9282015.

[19] L. Zhang, Z. Zhang, J. Qin, D. Shi, and Z. Wang, "Design and Performance Evaluation of the Modular Multilevel Converter (MMC)-based Grid-tied PV-Battery Conversion System," in *2018 IEEE Energy Conversion Congress and Exposition (ECCE)*, 23-27 Sept. 2018 2018, pp. 2649-2654, doi: 10.1109/ECCE.2018.8558443.

[20] J. Echeverría, S. Kouro, M. Pérez, and H. Abu-rub, "Multi-modular cascaded DC-DC converter for HVDC grid connection of large-scale photovoltaic power systems," in *IECON 2013 - 39th Annual Conference of the IEEE Industrial Electronics Society*, 10-13 Nov. 2013 2013, pp. 6999-7005, doi: 10.1109/IECON.2013.6700293.

[21] M. Alsadah and F. Mancilla-David, "Modeling and control of grid-connected photovoltaic power plants utilizing a simplified model of the modular multilevel converter," in *2014 North American Power Symposium (NAPS)*, 7-9 Sept. 2014 2014, pp. 1-6, doi: 10.1109/NAPS.2014.6965433.

[22] S. Rivera, B. Wu, R. Lizana, S. Kouro, M. Perez, and J. Rodriguez, "Modular multilevel converter for large-scale multistring photovoltaic energy conversion system," in *2013 IEEE Energy Conversion Congress and Exposition*, 15-19 Sept. 2013 2013, pp. 1941-1946, doi: 10.1109/ECCE.2013.6646945.

[23] D. Tiku, "Modular multilevel MMI (HB) topology for single-stage grid connected PV plant," in *11th IET International Conference on AC and DC Power Transmission*, 2015: IET, pp. 1-8.

[24] F. Rong, X. Gong, and S. Huang, "A Novel Grid-Connected PV System Based on MMC to Get the Maximum Power Under Partial Shading Conditions," *IEEE Transactions on*

Power Electronics, vol. 32, no. 6, pp. 4320-4333, 2017, doi: 10.1109/TPEL.2016.2594078.

[25] H. Bayat and A. Yazdani, "A Hybrid MMC-Based Photovoltaic and Battery Energy Storage System," *IEEE Power and Energy Technology Systems Journal*, vol. 6, no. 1, pp. 32-40, 2019, doi: 10.1109/JPETS.2019.2892418.

[26] A. B. Acharya, L. E. Norum, and D. Sera, "A Shadow Tolerant Configuration for PV Integration to Grid using Modular Multilevel Converter," in *2018 IEEE International Conference on Power Electronics, Drives and Energy Systems (PEDES)*, 18-21 Dec. 2018 2018, pp. 1-6, doi: 10.1109/PEDES.2018.8707829.

[27] *IEEE Recommended Practice and Requirements for Harmonic Control in Electric Power Systems*, 2014.

[28] K. Ilves, A. Antonopoulos, S. Norrga, and H. P. Nee, "Steady-State Analysis of Interaction Between Harmonic Components of Arm and Line Quantities of Modular Multilevel Converters," *IEEE Transactions on Power Electronics*, vol. 27, no. 1, pp. 57-68, 2012, doi: 10.1109/TPEL.2011.2159809.

[29] T. Qingrui, X. Zheng, H. Huang, and Z. Jing, "Parameter design principle of the arm inductor in modular multilevel converter based HVDC," in *2010 International Conference on Power System Technology*, 24-28 Oct. 2010 2010, pp. 1-6, doi: 10.1109/POWERCON.2010.5666416.

[30] J. Wang *et al.*, "Cycle-life model for graphite-LiFePO4 cells," *Journal of Power Sources*, vol. 196, no. 8, pp. 3942-3948, 2011/04/15/ 2011, doi: //10.1016/j.jpowsour.2010.11.134.

[31] N. Omar *et al.*, "Lithium iron phosphate based battery – Assessment of the aging parameters and development of cycle life model," *Applied Energy*, vol. 113, pp. 1575-1585, 2014/01/01/ 2014, doi: https://doi.org/10.1016/j.apenergy.2013.09.003.

[32] J. Hurtt and K. Baker, "Minimum Battery Energy Storage System Sizing Integrated with a Photovoltaic Plant Considering Practical Limitations," 2021: IEEE, doi:

10.1109/powertech46648.2021.9494981. [Online]. Available: https://dx.doi.org/10.1109/powertech46648.2021.9494981

[33] M. J. E. Alam and T. K. Saha, "Cycle-life degradation assessment of Battery Energy Storage Systems caused by solar PV variability," in *2016 IEEE Power and Energy Society General Meeting (PESGM)*, 17-21 July 2016 2016, pp. 1-5, doi: 10.1109/PESGM.2016.7741532.

[34] M. Musallam and C. M. Johnson, "An Efficient Implementation of the Rainflow Counting Algorithm for Life Consumption Estimation," *IEEE Transactions on Reliability*, vol. 61, no. 4, pp. 978-986, 2012, doi: 10.1109/TR.2012.2221040.

[35] M. Chawla, R. Naik, R. Burra, and H. Wiegman, "Utility energy storage life degradation estimation method," in *2010 IEEE Conference on Innovative Technologies for an Efficient and Reliable Electricity Supply*, 27-29 Sept. 2010 2010, pp. 302-308, doi: 10.1109/CITRES.2010.5619790.

[36] M. Ecker *et al.*, "Calendar and cycle life study of Li(NiMnCo)O2-based 18650 lithium-ion batteries," *Journal of Power Sources*, vol. 248, pp. 839-851, 2014/02/15/ 2014, doi: 10.1016/j.jpowsour.2013.09.143.

[37] S. Du, J. Liu, and T. Liu, "Modulation and Closed-Loop-Based DC Capacitor Voltage Control for MMC With Fundamental Switching Frequency," *IEEE Transactions on Power Electronics*, vol. 30, no. 1, pp. 327-338, 2015, doi: 10.1109/TPEL.2014.2301836.

[38] A. Lesnicar and R. Marquardt, "An innovative modular multilevel converter topology suitable for a wide power range," in *2003 IEEE Bologna Power Tech Conference Proceedings*, 23-26 June 2003 2003, vol. 3, p. 6 pp. Vol.3, doi: 10.1109/PTC.2003.1304403.

[39] Y. Xu, H. Xiao, Z. Xu, Y. Lu, J. Li, and P. Qiu, "Capacitor Voltage Balancing Algorithm Using Voltage Fluctuation Threshold for Modular Multilevel Converters," in *2018 IEEE/PES Transmission and Distribution Conference and Exposition (T&D)*, 16-19 April 2018 2018, pp. 1-9, doi: 10.1109/TDC.2018.8440444.

[40] S. Rohner, S. Bernet, M. Hiller, and R. Sommer, "Modulation, Losses, and Semiconductor Requirements of Modular Multilevel Converters," *IEEE Transactions on Industrial Electronics*, vol. 57, no. 8, pp. 2633-2642, 2010, doi: 10.1109/TIE.2009.2031187.

[41] W. Li, L. Grégoire, and J. Bélanger, "A Modular Multilevel Converter Pulse Generation and Capacitor Voltage Balance Method Optimized for FPGA Implementation," *IEEE Transactions on Industrial Electronics*, vol. 62, no. 5, pp. 2859-2867, 2015, doi: 10.1109/TIE.2014.2362879.

[42] G. Chen, H. Peng, R. Zeng, Y. Hu, and K. Ni, "A Fundamental Frequency Sorting Algorithm for Capacitor Voltage Balance of Modular Multilevel Converter With Low-Frequency Carrier Phase Shift Modulation," *IEEE Journal of Emerging and Selected Topics in Power Electronics*, vol. 6, no. 3, pp. 1595-1604, 2018, doi: 10.1109/JESTPE.2017.2764684.

[43] M. Hagiwara and H. Akagi, "PWM control and experiment of modular multilevel converters," in *2008 IEEE Power Electronics Specialists Conference*, 15-19 June 2008 2008, pp. 154-161, doi: 10.1109/PESC.2008.4591917.

[44] L. Luo, Y. Zhang, L. Jia, and N. Yang, "Capacitor voltage balancing method for modified modular multilevel converter," *IEEJ Transactions on Electrical and Electronic Engineering*, vol. 13, no. 8, pp. 1142-1152, 2018.

[45] H. Akagi, "Classification, Terminology, and Application of the Modular Multilevel Cascade Converter (MMCC)," *IEEE Transactions on Power Electronics*, vol. 26, no. 11, pp. 3119-3130, 2011, doi: 10.1109/TPEL.2011.2143431.

[46] M. Hagiwara and H. Akagi, "Control and Experiment of Pulsewidth-Modulated Modular Multilevel Converters," *IEEE Transactions on Power Electronics*, vol. 24, no. 7, pp. 1737-1746, 2009, doi: 10.1109/TPEL.2009.2014236.

[47] H. Akagi, "Multilevel Converters: Fundamental Circuits and Systems," *Proceedings of the IEEE*, vol. 105, no. 11, pp. 2048-2065, 2017, doi: 10.1109/JPROC.2017.2682105.

[48] H. A. Li and R. H. G. Tan, "Performance Evaluation of BESS Moving Average Control for 1MW PV Plant," in *2021 Innovations in Power and Advanced Computing Technologies (i-PACT)*, 27-29 Nov. 2021 2021, pp. 1-8, doi: 10.1109/i-PACT52855.2021.9696827.

[49] R. P. Sasmal, S. Sen, and A. Chakraborty, "Solar photovoltaic output smoothing: Using battery energy storage system," in *2016 National Power Systems Conference (NPSC)*, 19-21 Dec. 2016 2016, pp. 1-5, doi: 10.1109/NPSC.2016.7858894.

[50] B. Schnierer. "Maldives - Solar Radiation Measurement Data." https://energydata.info/dataset/maldives-solar-radiation-measurement-data (accessed June 7, 2022).